



HAL
open science

Experimental and modeling study of the oxidation of n-butylbenzene

Benoit Husson, Roda Bounaceur, Kotaro Tanaka, Maude Ferrari, Olivier Herbinet, Pierre Alexandre Glaude, René Fournet, Frédérique Battin-Leclerc, Moïse Crochet, Guillaume Vanhove, et al.

► **To cite this version:**

Benoit Husson, Roda Bounaceur, Kotaro Tanaka, Maude Ferrari, Olivier Herbinet, et al.. Experimental and modeling study of the oxidation of n-butylbenzene. *Combustion and Flame*, 2012, 159 (4), pp.1399-1416. 10.1016/j.combustflame.2011.12.006 . hal-00726401

HAL Id: hal-00726401

<https://hal.science/hal-00726401>

Submitted on 30 Aug 2012

HAL is a multi-disciplinary open access archive for the deposit and dissemination of scientific research documents, whether they are published or not. The documents may come from teaching and research institutions in France or abroad, or from public or private research centers.

L'archive ouverte pluridisciplinaire **HAL**, est destinée au dépôt et à la diffusion de documents scientifiques de niveau recherche, publiés ou non, émanant des établissements d'enseignement et de recherche français ou étrangers, des laboratoires publics ou privés.

Experimental and modeling study of the oxidation of *n*-butylbenzene

B. Husson^a, R. Bounaceur^a, K. Tanaka^a, M. Ferrari^a, O. Herbinet^a, P.A. Glaude^a, R. Fournet^a, F. Battin-Leclerc^a, M. Crochet^b, G. Vanhove^b, R. Minetti^b, C.J. Tobin^c, K. Yasunaga^c, J.M. Simmie^c, H.J. Curran^c, T. Niass^d, O. Mathieu^d, S.S. Ahmed^d

^a *Laboratoire Réactions et Génie des Procédés, CNRS, Université de Lorraine, 1 rue Grandville, BP 451, 54001 Nancy Cedex, France*

^b *Physico-Chimie des processus de Combustion et de l'atmosphère (PC2A), CNRS, Université des Sciences et Technologies de Lille, Bâtiment C11, 59655 Villeneuve d'Ascq Cedex, France*

^c *Combustion Chemistry Centre (C3), National University of Ireland, Galway, Ireland*

^d *Saudi-Aramco, Research & Development Center, P.O. Box 1657, Dhahran 31311, Saudi Arabia*

Abstract

New experimental results for the oxidation of *n*-butylbenzene, a component of diesel fuel, have been obtained using three different devices. A rapid compression machine has been used to measure autoignition delay times after compression at temperatures in the range 640–960 K, at pressures from 13 to 23 bar, and at equivalence ratios from 0.3 to 0.5. Results show low-temperature behavior, with the appearance of cool flames and a negative temperature coefficient (NTC) region for the richest mixtures. To investigate this reaction at higher temperatures, a shock tube has been used. The shock tube study was performed over a wide range of experimental temperatures, pressures, and equivalence ratios, with air used as the fuel diluent. The ignition temperatures were recorded over the range 980–1740 K, at reflected shock pressures of 1, 10, and 30 atm. Mixtures were investigated at equivalence ratios of 0.3, 0.5, 1.0 and 2.0 in order to determine the effects of fuel concentration on reactivity over the entire temperature range. Using a jet-stirred reactor, the formation of numerous reaction products has been followed at temperatures from 550 to 1100 K, at atmospheric pressure, and at equivalence ratios of 0.25, 1.0, and 2.0. Slight low-temperature reactivity (below 750 K) with a NTC region has been observed, especially for the leanest mixtures. A detailed chemical kinetic model has been written based on rules similar to those considered for alkanes by the system EXGAS developed at Nancy. Simulations using this model have been compared to the experimental results presented in this study, but also to results in the literature obtained in a jet-stirred reactor at 10 bar, in the same rapid compression machine for stoichiometric mixtures, in a plug flow reactor at 1069 K and atmospheric pressure, and in a low-pressure (0.066 bar) laminar premixed methane flame doped with *n*-butylbenzene. The observed agreement is globally better than that obtained with models from the literature. Flow rate and sensitivity analyses have revealed a preponderant role played by the addition to molecular oxygen of resonantly stabilized, 4-phenylbut-4-yl radicals.

Corresponding Author:

Frédérique Battin-Leclerc
Laboratoire Réactions et Génie des Procédés
Ecole Nationale Supérieure des Industries Chimiques
BP 20451, 1 rue Grandville, 54000 Nancy, France
Tel: +33 (0)3 83 17 51 25
Fax: +33 (0)3 83 17 81 20
E-mail: Frederique.Battin-Leclerc@ensic.inpl-nancy.fr

Keywords: *n*-Butylbenzene; Jet-stirred reactor; Rapid compression machine; Shock tube; Gas-phase oxidation; Detailed chemical model

1. Introduction

Continuous improvements in engine efficiency and emissions are needed to meet future strict emission and fuel consumption regulations. Such improvements can only be obtained through a good understanding of the chemistry of fuel oxidation. Among automotive fuels, diesel fuel is a complex mixture consisting of alkanes (approximately 30% by mass), alkylcyclohexanes (approximately 24%), alkyldecalines (approximately 15%), alkylbenzenes (approximately 10%), and polycyclic naphthenoaromatic compounds, which contain from 10 to 20 carbon atoms [1]. As it is difficult to consider the oxidation chemistry of all diesel fuel components because of the complexity of the composition of these mixtures, surrogate fuels have been suggested: e.g., a mixture of *n*-hexadecane, heptamethylnonane, *n*-decylbenzene, and 1-methylnaphthalene [2]. Although the oxidation of alkanes has been well studied, there have not been many studies of the oxidation mechanisms of cycloalkanes, alkylbenzenes, and polycyclic aromatic compounds [3].

Before undertaking the study of alkylbenzenes with a large side chain, such as *n*-decylbenzene, as proposed by Farrell et al. [2], it is first necessary to investigate the oxidation of alkylbenzenes with smaller side chains (from two to four atoms of carbon). The high-temperature (above 900 K) oxidation of these compounds has already been investigated in several systems. Premixed flames of ethylbenzene [4] and [5] and nonpremixed methane flames doped with ethylbenzene, propylbenzene, and butylbenzene [6] have been studied. The structure of a laminar premixed methane flame doped with *n*-butylbenzene [7] has also been investigated. The oxidation of the several alkylbenzenes with side chains from C₂ to C₄ has been studied in a flow reactor [8], [9], [10] and [11] for temperatures between 1000 and 1200 K. The oxidation of *n*-propylbenzene has been investigated in a jet-stirred reactor [12] for temperatures between 900 and 1250 K. Note that no data have been published on the high-temperature ignition of alkylbenzenes larger than ethylbenzene [13] and *n*-propylbenzene [14].

Recent results concerning the low-temperature oxidation of these compounds are even scarcer. The autoignition of alkylbenzenes with small side chains, such as isomers of xylenes or *n*-butylbenzene, has been investigated in a rapid compression machine in Lille at temperatures from 600 to 900 K for stoichiometric mixtures [15] and [16]. According to Roubaud et al. [15], alkylbenzenes can be divided into two groups according to their autoignition characteristics. The compounds in the first group present features of low-temperature reactivity such as a negative temperature coefficient (NTC) zone: *o*-xylene, 1,2,3-trimethylbenzene, propylbenzene, and *n*-butylbenzene. The compounds in the other group do not present these features: toluene, and *m*- and *p*-xylene. A mechanism was proposed by Ribaucour et al. [16] to simulate the autoignition of *n*-butylbenzene in a rapid compression machine. The oxidation of *n*-butylbenzene has recently been studied in a jet-stirred reactor [17] in the temperature range 550–1150 K, at 10 bar, for equivalence ratios from 0.25 to 1.5, and at a residence time of 1 s. In these experiments, only very low reactivity was observed below 800 K, even for the leanest mixtures, because of the very large dilution (0.1% initial fuel mole fraction) used in this study. These results have been simulated [17] using a model based on that of Ribaucour et al. [16].

The purpose of the present paper is to thoroughly investigate the autoignition and the low-temperature oxidation of *n*-butylbenzene. New autoignition results have been obtained in a rapid compression machine at temperatures from 640 to 960 K for lean mixtures (Φ from 0.3 to 0.5), as well as in a shock tube at temperatures from 980 to 1740 K, for lean to rich mixtures (Φ from 0.3 to 2.0), and at pressures of 1, 10, and 30 atm. New data have also been obtained for oxidation in a

jet-stirred reactor (temperatures from 550 to 1100 K) at atmospheric pressure, but with a higher fuel initial mole fraction (0.4%) and a longer residence time (2 s) compared to [17]. A new mechanism has been proposed based on recent work on the oxidation of alkanes [18], alkenes [19], aromatic compounds [20], and other modeling studies of the oxidation of large surrogates for diesel and biodiesel fuels [21] and [22].

2. Experimental methods and results

Three experimental facilities have been used: a rapid compression machine (RCM), a shock tube (ST), and a jet-stirred reactor (JSR). Tables presenting the experimental data recorded are available as Supplementary material.

2.1. Rapid compression machine experiments

Autoignition delays were measured in the RCM facility in Lille University, following the procedure discussed previously [23]. Pure nitrogen, carbon dioxide, and argon, as well as mixtures of them, were used as inert gases to span a compressed-gas temperature range of 640–960 K. The adiabatic core gas temperature (T_C) is calculated from the initial pressure (P_0) and temperature (T_0), the compressed pressure (P_C), which can be experimentally measured at top dead center and the ratio of specific heats ($\gamma = C_p/C_v$), using the following equation [24]:

$$\int_{T_0}^{T_C} \frac{\gamma}{(\gamma - 1) T} dT = \ln \frac{P_C}{P_0}$$

P_C is varied by modifying the initial charge. The cool flame delay time is measured from the time when the piston reaches TDC to the maximum of the first peak of light emission. The ignition delay time is measured from the time at TDC to the point of intersection of two lines: one line tangent to the portion of the pressure signal marked by the pressure rise associated with ignition, and the other tangent to the portion of the pressure signal before the pressure rise. This procedure was used because the pressure rise was often not sharp, due to the low equivalence ratio, and because it does not interfere with the usual definition of the ignition time when the pressure rise is sharp. The uncertainty in the in-cylinder pressure was limited by the resolution of the data acquisition system used for these experiments. This and the uncertainty in the measurement of the initial pressure lead to an uncertainty in the calculated adiabatic core gas temperature T_C that is less than 1%. Severe fluid motion during and after compression was avoided by using a relatively long compression time of 60 ms.

Lean *n*-butylbenzene/O₂/inert mixtures were prepared inside glass vessels, following the partial pressures method, and left to homogenize overnight. Two sets of data were obtained, one with an equivalence ratio of $\Phi = 0.5$ and dilution as in air, and another for three equivalence ratios ($\Phi = 0.3, 0.4, 0.5$) for which the dilution by the inert gas was reduced to a molar ratio of [oxygen]/[inert] = 0.37 to facilitate ignition and ensure that the ignition delays measured were inside the domain of validity of the RCM, as in a previous study on aromatics [15]. The gas mixture preparation facility was heated to 353 K to ensure sufficient vapor pressure, since *n*-butylbenzene has a low boiling point. The low volatility of this aromatic compound explains why it was not possible to reach the vapor pressures corresponding to rich mixtures without heating the mixture to higher temperatures, with risks of fuel degradation. The maximum partial pressure of *n*-butylbenzene in the mixtures was 1300 Pa, which is well below its vapor pressure of 3100 Pa at 353 K. The temperature along the gas lines that lead to the RCM was monitored to make sure no cold spots were present. The combustion chamber of the RCM was heated to 363 K. *n*-Butylbenzene used in the experiments was 99+% pure and was bought from Aldrich Chemicals. It was further purified from dilute air by several freeze–pump–thaw cycles.

The pressure at the end of compression, PTDC, varied from 1.33 to 2.29 MPa. In-cylinder pressure and light emission profiles were recorded with a 40- μ s time step during each experiment to measure the total and cool-flame ignition delay times.

In Fig. 1 and Fig. 2, symbols correspond to experimental results and lines to simulations. The figures present the experimental ignition delay times obtained for three equivalence ratios (Φ), 0.3, 0.4, and 0.5, and for three initial pressures (P_0), 0.093, 0.106, and 0.120 MPa (700, 800, and 900 Torr). For the three equivalence ratios, ignition delay times at a given temperature decrease with increasing pressure. The very lean mixtures exhibit very low reactivity with no ignition below 700 K, even for the highest pressures, and no NTC behavior.

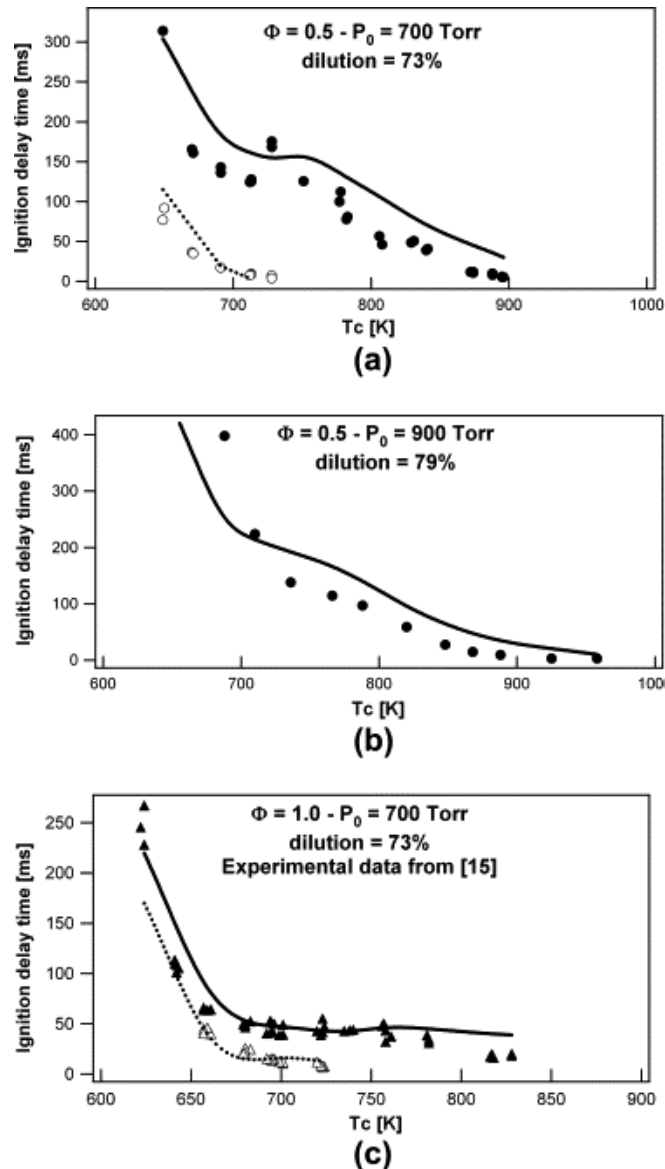


Fig. 1. Rapid compression machine: experimental and computed delay times versus compressed gas temperature for *n*-butylbenzene/oxygen/nitrogen/argon/carbon dioxide mixtures with $\Phi = 0.5$ at PTDC from 13.4 to 16.6 bar (initial pressure of 700 Torr) and at PTDC from 17.2 to 23.2 bar (initial pressure of 900 Torr) and $\Phi = 1$ (experiments from [15]) at PTDC from 13.4 to 17.9 bar (initial pressure of 700 Torr). Points are experiments and lines simulations. The black symbols and full lines correspond to main ignition, the white points and dotted lines to cool flame.

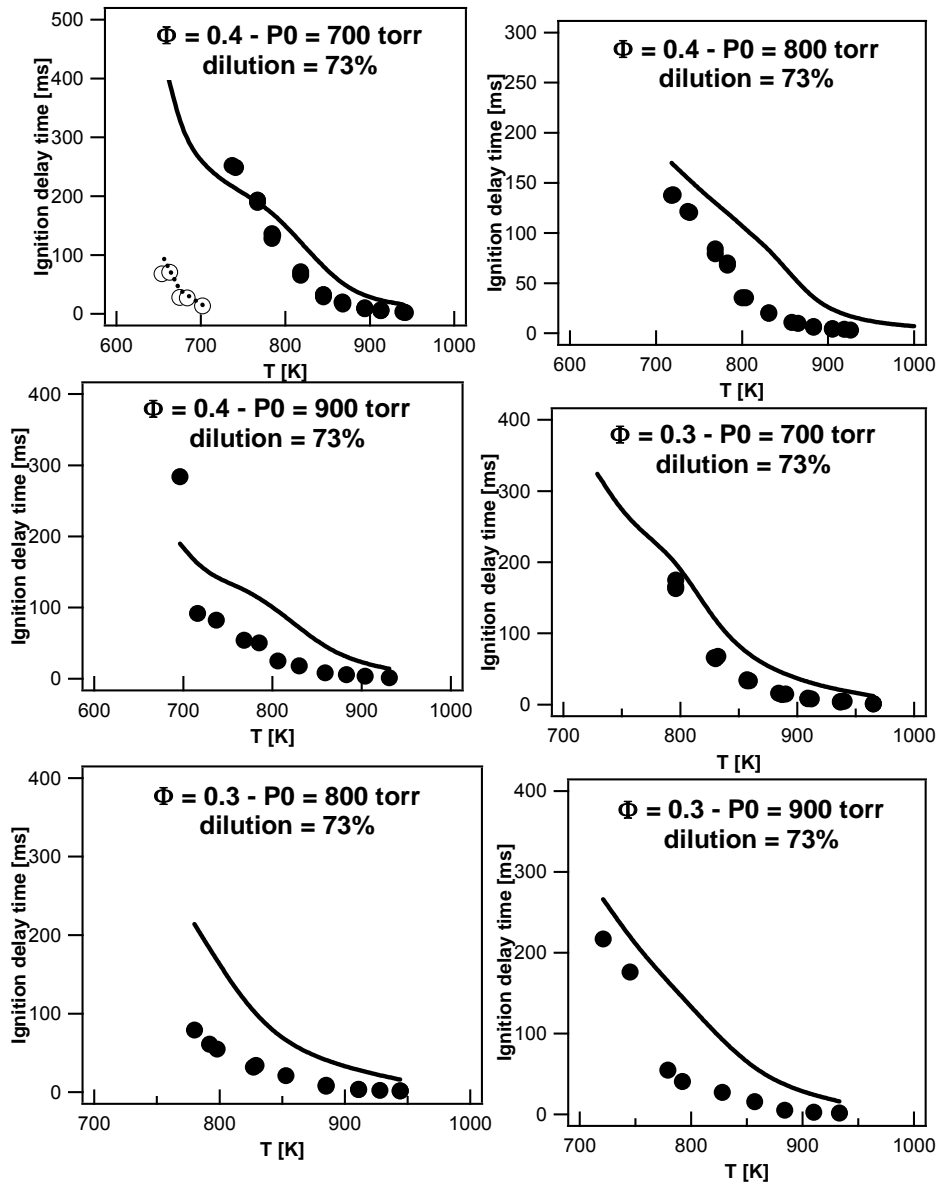


Fig. 2. Rapid compression machine: experimental and computed delay times versus compressed gas temperature for n-butylbenzene/oxygen/nitrogen/argon/carbon dioxide mixtures with $\Phi = 0.4$ at PTDC from 14.3 to 18.3 bar (initial pressure of 700 Torr), PTDC from 16.3 to 21.0 bar (initial pressure of 800 Torr), and PTDC from 17.9 to 23 bar (initial pressure of 900 Torr), and $\Phi = 0.3$ at PTDC from 15.6 to 18.8 bar (initial pressure of 700 Torr), PTDC from 17.5 to 20.0 bar (initial pressure of 800 Torr), and PTDC from 17.9 to 23.0 bar (initial pressure of 900 Torr). Points are experiments and lines simulations. The black points and full lines correspond to main ignition, the white points and dotted lines to cool flame.

Figure 1 displays the results obtained for $\Phi = 0.5$ and $P_0 = 700$ and 900 Torr. A zone of NTC is observed, as well as cool flames below 740 K. For comparison, Fig. 1c also presents the results previously obtained by Roubaud et al. [15] for a stoichiometric mixture using the same apparatus and the same initial pressure; a higher reactivity is observed, with an NTC zone and the appearance of cool flames. Figure 2 shows the results obtained for the two leanest mixtures with equivalence ratios of 0.3 and 0.4. The reactivity of these mixtures is lower than for $\Phi = 0.5$, with no NTC zone, nor are cool flames observed (except at $\Phi = 0.4$ for $P_0 = 700$ Torr).

Stable products formed during the ignition delay were sampled by rapid quenching of the whole reacting mixture inside a sampling vessel. The sampling system has a characteristic time for the pressure to fall to 50% of its initial value of 2 ms. Because all of the combustion chamber volume is sampled during this process, sampling times are very accurately recorded using the pressure profile. Samples have been taken 30 ms after compression, under the following conditions: PTDC = 1.4 MPa, $T_c = 690$ K, $\Phi = 0.5$. Under these conditions, the cool flame delay time was 16 ms, and the total ignition delay time was 130 ms. Corresponding samples were analyzed by gas chromatography using HP-5 column, as well as mass spectrometry, a thermal conductivity detector (TCD), and a flame ionization detector (FID), allowing identification and quantification of the heavy products formed during the cool flame. Under these conditions, the conversion of *n*-butylbenzene was 17% and the main aromatic products were styrene (with a carbon atom selectivity of 42%; i.e., 42% of the initial carbon atoms present as *n*-butylbenzene are converted to styrene), benzaldehyde (with a selectivity of 22%), but-2-enylbenzene (with a carbon atom selectivity of 13%) and but-3-enylbenzene (with a carbon atom selectivity of 6.5%). Table 1 presents the name and formula of the C₁₀ aromatic products identified. Among the products listed in Table 1, only butenylbenzenes have been quantified. However, several oxygenated products have been detected, such as aromatic cyclic ethers.

Table 1. Name and formula of the C₁₀ aromatic products identified.

Name	Formula	Name	Formula
but-2-enylbenzene		but-3-enylbenzene	
but-2,4dienylbenzene		1,2,3,4-tetrahydronaphthalene	
1-phenylbutan-2-one		1-phenylbutan-1-one	
3-phenyltetrahydrofuran		2-benzyl-3-methyloxirane	
2-ethyl-3-phenyloxirane			

Note: Sampling performed 30 ms after compression, under the following conditions: PTDC = 1.4 MPa, $T_c = 675$ K, $\Phi = 0.5$.

2.2. Shock tube experiments

The high-pressure shock tube consists of a driver section 3 m in length and a driven section 5.73 m in length. The internal diameter is 6.3 cm and both sections are made of stainless steel. Between these sections is a double diaphragm section that consists of two polyethylene terephthalate plastic diaphragms (Katco Ltd.) of varying thickness (75–500 μm) depending on the shock pressures one aims to achieve. Helium was used as the driver gas, which eventually bursts the diaphragms as a

result of a large pressure differential between the driver and driven sections. This bursting of the diaphragms leads to a shock wave that compresses the fuel in the driven section.

At the endplate section there are four piezoelectric pressure transducers (PCB 113A24) at distances of 0, 9.9, 20, and 50 cm from the endplate. These transducers allow the measurement of the incident shock velocity using two Fluke PM6681 high-resolution counters and one Phillips PM6666 programmable counter. The transducers also allow the measurement of reflected shock conditions (p_5 , T_5) by inputting the incident shock velocity and initial temperature and pressure into the computer program GasEq [25]. The accuracy of T_5 is ± 15 K. At the pressure transducer 0 cm from the endplate there was an optical window in the center where there was a photodiode detector (Thor lab) to detect light emission. The ignition delay time was measured on a digital oscilloscope workstation (Sigma) between the pressure increase as a result of compression and the maximum rate of pressure increase as a result of ignition. The accuracy of the ignition delay time is about 15%.

2.2.1. Heating system

A heating system was designed and installed on the driven section, manifold, and mixing tanks to ensure that the low-vapor-pressure fuel, whose saturation vapor pressure is 9.3 kPa [26] at 373 K, was present in the gas phase for the duration of the experiment and that no condensation of the fuel occurred.

A series of heating tapes (1250 W, Flexelec), thermostats (16 A, Flexelec and 2 A, Vulcanic-30633), thermocouples, and insulation tape (Zetex 1000, Final) were used to heat the shock tube, manifold, and mixing tanks, while a thermometer digital output coupled with sensors was used to monitor the temperatures. The temperature of the shock tube walls was maintained at 393 K during experimentation to eliminate the possibility of fuel condensation. For a more in-depth description of the heating system, refer to the paper by Darcy et al. [14].

2.2.2. Mixture preparation

The fuel mixture was prepared in a 79:21 ($N_2:O_2$) blend in two heated 50-L stainless steel tanks (Nor Cal), which were connected to the shock tube via the manifold. *n*-Butylbenzene was supplied by Tokyo Chemicals Ltd (purity > 99%). Oxygen (99.5%) and nitrogen (99.998%) were supplied by BOC. The driver gas was helium (99.99%; BOC). Mixtures were prepared via injection (compositions can be seen in the Supplementary section) and care was taken to ensure that the maximum fuel pressure utilized was half the vapor pressure (4.5 kPa) at which *n*-butylbenzene condenses under the experimental operating condition of 293 K. This ensured that there was minimal opportunity for the fuel to condense. The accuracy on the initial concentrations is approximately 10%. The driven section of the shock tube was cleaned before and after each day's experiments to ensure that all soot emitted postignition was removed from the shock tube, and thus preignition and contamination were avoided, particularly under rich conditions and high pressures, in which large quantities of fuel mixture were required to achieve reasonable ignition delay times.

Ignition delay times of *n*-butylbenzene were studied at equivalence ratios of 0.3, 0.5, 1.0, and 2.0. The percentage fuel corresponding to each equivalence ratio was 0.46%, 0.77%, 1.53%, and 3.02%, respectively. Experiments were carried out over a wide range of temperatures, 980–1750 K, and pressures 1, 10, and 30 atm. Figure 3 shows a typical pressure history.

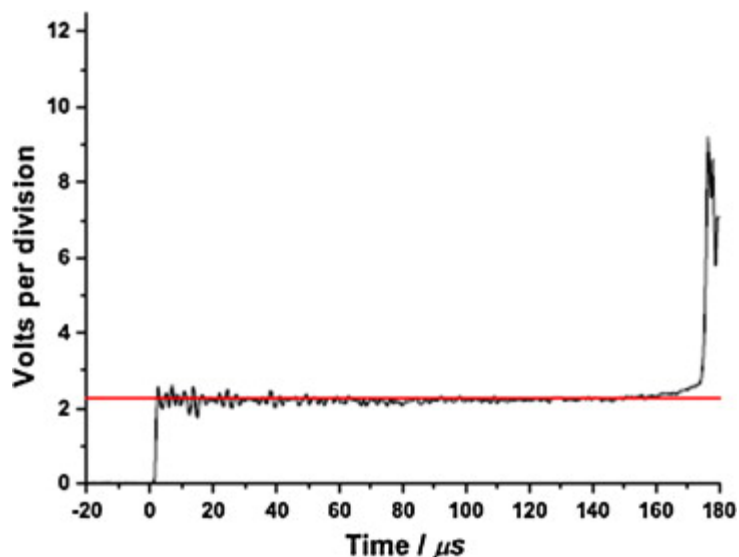


Fig. 3. Shock tube: a typical pressure trace obtained at an equivalence ratio of 0.3 at 30 atm pressure.

For organic compound/oxygen/argon mixtures, the determination of power dependences is often proposed from the overall statistical correlation between ignition delay times (τ) and gas concentrations. From the results obtained here for *n*-butylbenzene (BB), the following correlation was derived (concentrations are in mol cm⁻³):

$$\tau(\text{s}) = 9.13 \times 10^{-13} \exp(13,266/T) [\text{BB}]^{-0.159} [\text{O}_2]^{-1.493} [\text{Inert gas}]^{1.049}.$$

Figure 4 presents a comparison between ignition delay times in shock tube which can be derived from this correlation between 1000 and 1400 K (equivalence ratio of 0.5 and pressure of 20 bar) and the results measured in rapid compression machine at normal dilution (see Fig. 1b). A good agreement between both sources of ignition delay times is observed.

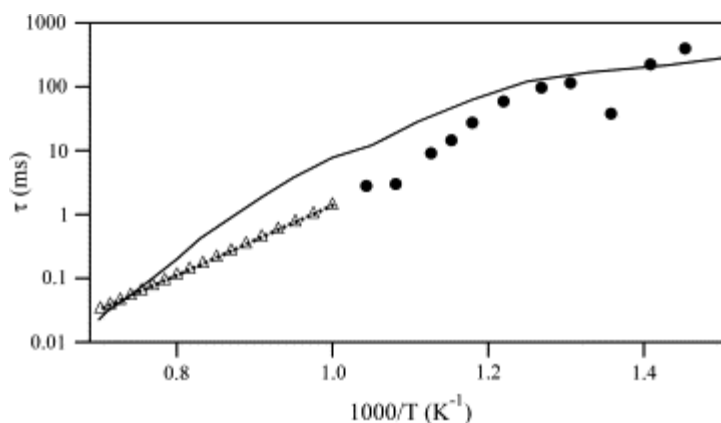


Fig. 4. Comparison between the experimental ignition delay times obtained in a rapid compression machine (symbols), the correlation derived from shock tube experiments (symbols with line), and simulations (line) for a pressure of 20 bar and an equivalence ratio of 0.5.

2.2.3. Influence of pressure on ignition delay times

The effect of pressure on ignition delay time was determined for all fuel mixtures. The observed trends in reactivity with pressure were very similar for all equivalence ratios; Mixtures studied at a reflected shock pressure of 1 atm were least reactive, followed by mixtures studied at 10 atm, with 30-atm experiments being fastest to ignite, see Fig. 5.

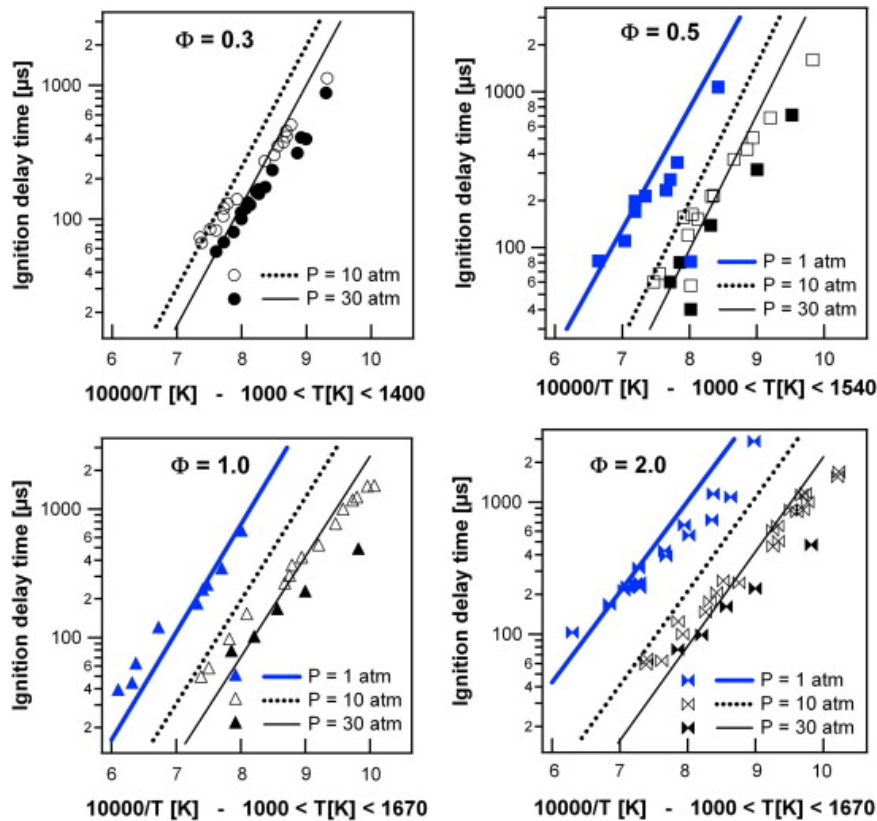


Fig. 5. Shock tube: effect of varying pressure on n-butylbenzene reactivity. Equivalence ratios of 0.3, 0.5, 1.0, and 2.0, respectively, at 1, 10, and 30 atm. Lines are model simulations.

While reactivity is directly related to pressure, the activation energies for the fuel-lean mixture ($\Phi = 0.3$), represented by the slope of the experimental data, do not vary significantly with pressure. The same trend is observed for all mixture compositions; see Fig. 5.

2.2.4. Influence of equivalence ratio on ignition delay times

The effect of equivalence ratio on ignition delay time was compared at 1, 10 and 30 atm. The experimental data corresponding to the four equivalence ratios cross over at increasing temperatures with increasing pressures; see Fig. 6. In the case of 30 atm, for which the studied temperature range was the lowest (980–1350 K), the fuel-rich mixture ($\Phi = 2$) is most reactive, whereas the fuel-lean mixture ($\Phi = 0.3$) is least reactive. The order of reactivity under these conditions is $\Phi = 2 > 1 > 0.5 > 0.3$. The opposite is true in the high-temperature region as it can be seen in the results at 1 atm over a temperature range (1165–1750 K): the fuel-lean mixture ($\Phi = 0.3$) is most reactive, whereas the fuel-rich mixture of 2.0 is least reactive. Reactivity in the high-temperature region is in the order $\Phi = 0.3 > 0.5 > 1 > 2$. At 10 atm, over the temperature range 975–1410 K, the influence of the equivalence ratio is not noticeable.

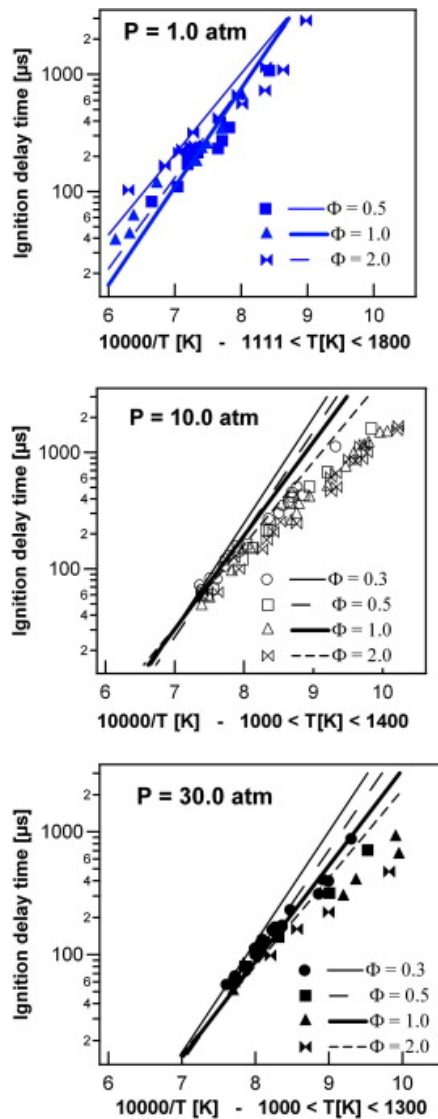


Fig. 6. Shock tube: effect of varying equivalence ratio on n-butylbenzene reactivity. The pressures were 1, 10, and 30 atm, respectively, at equivalence ratios of 0.3, 0.5, 1.0, and 2.0. Lines are model simulations.

The observed trends in reactivity were as expected; in the low-temperature region, the quantity of fuel present in the fuel mixture determines the reactivity, with the fuel-rich mixtures being most reactive. In this temperature region (1000–1200 K), the reaction which has the largest impact on the reactivity is the O_2 addition to the phenylbutyl radicals obtained from the fuel by H-atom abstractions. This reaction, which leads to peroxy radicals, drives a chain reaction (see further in the text) in which a sequence of hydrogen abstraction, chain branching, and chain propagation reactions lead to ignition. Note that the low-temperature reactivity is shifted toward higher temperature when pressure increases. This shift is due to the influence of pressure on the equilibrium of the addition reactions of molecular oxygen to the alkyl and hydroperoxyalkyl radicals.

In contrast, the quantity of O_2 present plays the most important role in the high-temperature region, where mixtures with the highest O_2 content (fuel-lean mixtures) are most reactive. High-temperature chemistry is dominated by the reaction of O_2 with a hydrogen radical, producing an oxygen atom and an hydroxyl radical. As usual for high-temperature ignition, this chain branching reaction drives the high temperature chemistry. Therefore, the leaner the mixture—the more oxygen present in the fuel mixture—the faster the chain-branching reaction between hydrogen radicals and oxygen molecules ($H + O_2 = O + OH$), and the higher the reactivity.

2.3. Jet-stirred reactor experiments

Mole fractions of reactants and products were measured as a function of temperature in the JSR facility of CNRS Nancy, following procedure discussed elsewhere [21] and [22]. The reactor was a fused silica jet-stirred reactor operated at constant temperature and pressure. It was composed of a sphere with an injection cross located at its center. The mixing of the gas phase inside the reactor was achieved through turbulent jets issued from the four nozzles of the cross. To avoid the formation of temperature gradients in the gas phase, the reactor is preceded by an annular pre-heater in which the temperature of the gas mixture is increased progressively to the reaction temperature. Despite the exothermicity of the reaction, the temperature gradient in the vessel was lower than 5 K. The liquid reactant flow rate was controlled using a liquid mass flow controller, mixed with the carrier gas, and then evaporated by passing through a single pass heat exchanger, the temperature of which was set above the boiling point of the mixture. Carrier gas and oxygen flow rates were controlled by gas mass flow controllers. The accuracy of liquid and gas mass flow rates is around 0.5%. The flow ranges of the mass flow controllers have limited the maximum concentration of fuel to 0.4%.

The oxidation of the *n*-butylbenzene was studied in the above-described reactor over the temperature range 550–1100 K, at a pressure of 106 kPa (800 Torr), at a residence time of 2 ± 0.02 s, for an inlet fuel mole fraction of 0.4% and equivalence ratios of 0.25, 1.0, and 2.0, with helium as the bath gas. *n*-Butylbenzene was purchased from Aldrich (purity > 99%). Helium and oxygen were provided by Messer (purity of 99.999% and of 99.995, respectively).

Reaction products were analyzed by gas chromatography. The analytical procedure has already been described in detail in a previous paper [22]. Analyzed species were light species such as oxygen, carbon monoxide, carbon dioxide, C₁–C₄ hydrocarbons, and small oxygenated compounds which were analyzed on line (Carbosphere column for O₂ and C₁–C₂ species, HP-Plot Q for C₃–C₄ species, TCD for O₂ and carbon oxides, FID for other species), as well as hydrocarbons and oxygenated species with more than five heavy atoms (carbon and oxygen atoms are considered as heavy atoms). The identification and the calibration of light species (e.g., carbon oxides, C₁–C₄ hydrocarbons) were performed by injecting gaseous samples provided by Messer and Air Liquide. Among the products that are known as important for hydrocarbon oxidation, only hydrogen, water, and formaldehyde were not quantified, but their presence was apparent in GC-MS analyses.

Heavy species were condensed in a trap maintained at liquid nitrogen temperature. After a given period of time, the trap was disconnected and acetone (solvent) and a known amount of *n*-octane acting as internal standard were added. When the temperature of the trap was close to room temperature, the liquid mixture in the trap was poured into a sampling bottle and then injected into a gas chromatograph (HP-5 column with FID). The identification of heavy hydrocarbons and oxygenated compounds was performed by comparison of retention times obtained by injecting pure substances when available. The identification was performed using a gas chromatograph coupled with a mass spectrometer (GC-MS) operating under the same conditions as the gas chromatograph used for the quantification, enabling the direct comparison of the two chromatograms. The quantification was obtained by comparing peak areas with that of *n*-octane. The calibration was performed by injecting known amounts of the pure substances when available; otherwise the method of effective carbon atoms was used (species having the same number of carbon atoms and the same functional groups were assumed to have the same response in the FID). The limit of detection was about 100 ppb for the heaviest species (FID) and about 10 ppm for carbon oxides and oxygen (TCD). Uncertainty estimates were about $\pm 5\%$ for species that are analyzed on line and $\pm 10\%$ for species condensed in the trap.

The formation of numerous reaction products was observed during the oxidation of *n*-butylbenzene. The evolution of the mole fractions of the reactants and of these products were recorded as a function of temperature (Fig. 7, Fig. 8 and Fig. 9). These species are

- Carbon oxides.
- Saturated hydrocarbons: methane and ethane.
- Olefins: ethylene, propene, and 1-butene.
- Poly-unsaturated hydrocarbons: acetylene, propyne, allene, and 1,3-butadiene.
- Aldehydes, ketones, cyclic ethers, and alcohols (including aromatic ones): acetaldehyde, acrolein, propanal, benzaldehyde, benzofuran, phenol, benzeneacetaldehyde, 2-methylphenol, and acetophenone.
- Aromatic compounds: benzene, toluene, ethylbenzene, styrene, 1-propenylbenzene, 2-propenylbenzene, indane, indene, 1-butenylbenzene, 2-butenylbenzene, 3-butenylbenzene, tetrahydro-naphthalene, 1,4-dihydronaphthalene, and naphthalene.

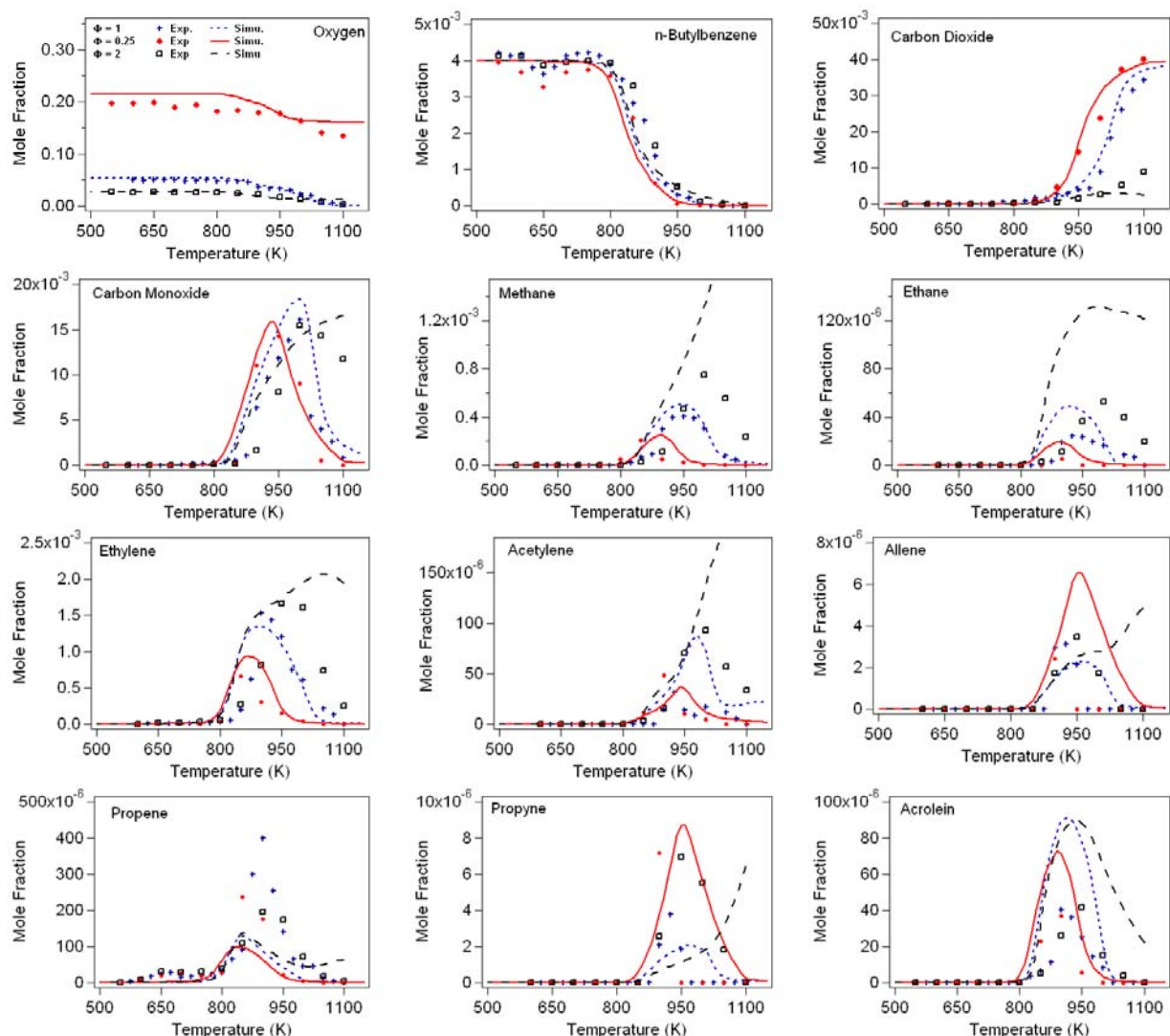


Fig. 7. Jet-stirred reactor ($P = 1.06$ bar): experimental and simulated mole fractions versus temperature for *n*-butylbenzene/oxygen/argon mixtures oxidation at a residence time of 2 s and for an inlet fuel mole fraction of 0.4% and equivalence ratios from 0.25 to 2. Points are experiments and lines simulations. $\Phi = 0.25$: circles and full line; $\Phi = 1$: cross and broken line; $\Phi = 2$: squares and large broken line.

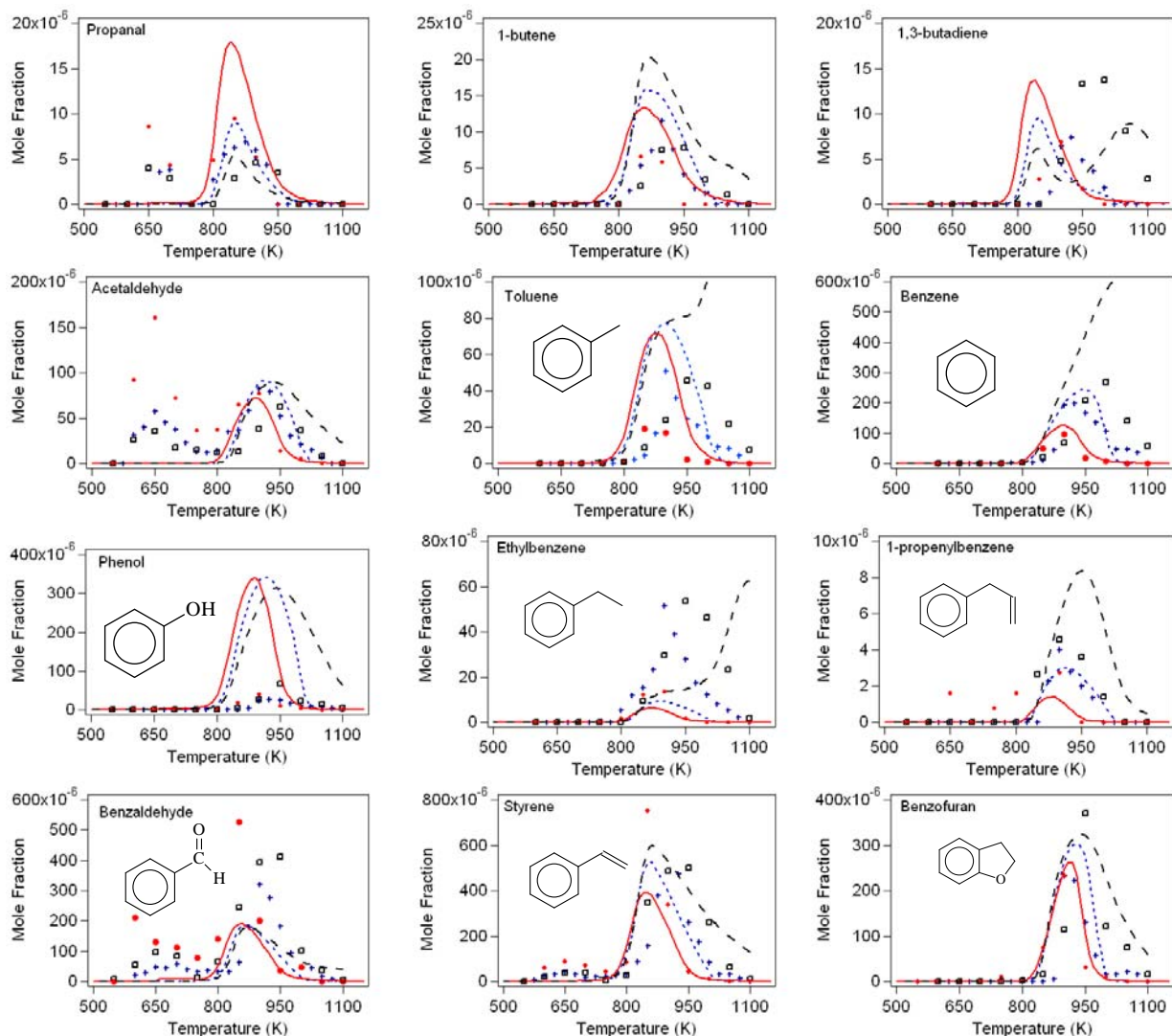


Fig. 8. Jet-stirred reactor ($P = 1.06$ bar): experimental and simulated mole fractions versus temperature for n-butylbenzene/oxygen/argon mixtures oxidation at a residence time of 2 s and for an inlet fuel mole fraction of 0.4% and equivalence ratios from 0.25 to 2. Points are experiments and lines simulations. $\Phi = 0.25$: circles and full line; $\Phi = 1$: cross and broken line; $\Phi = 2$: squares and large broken line.

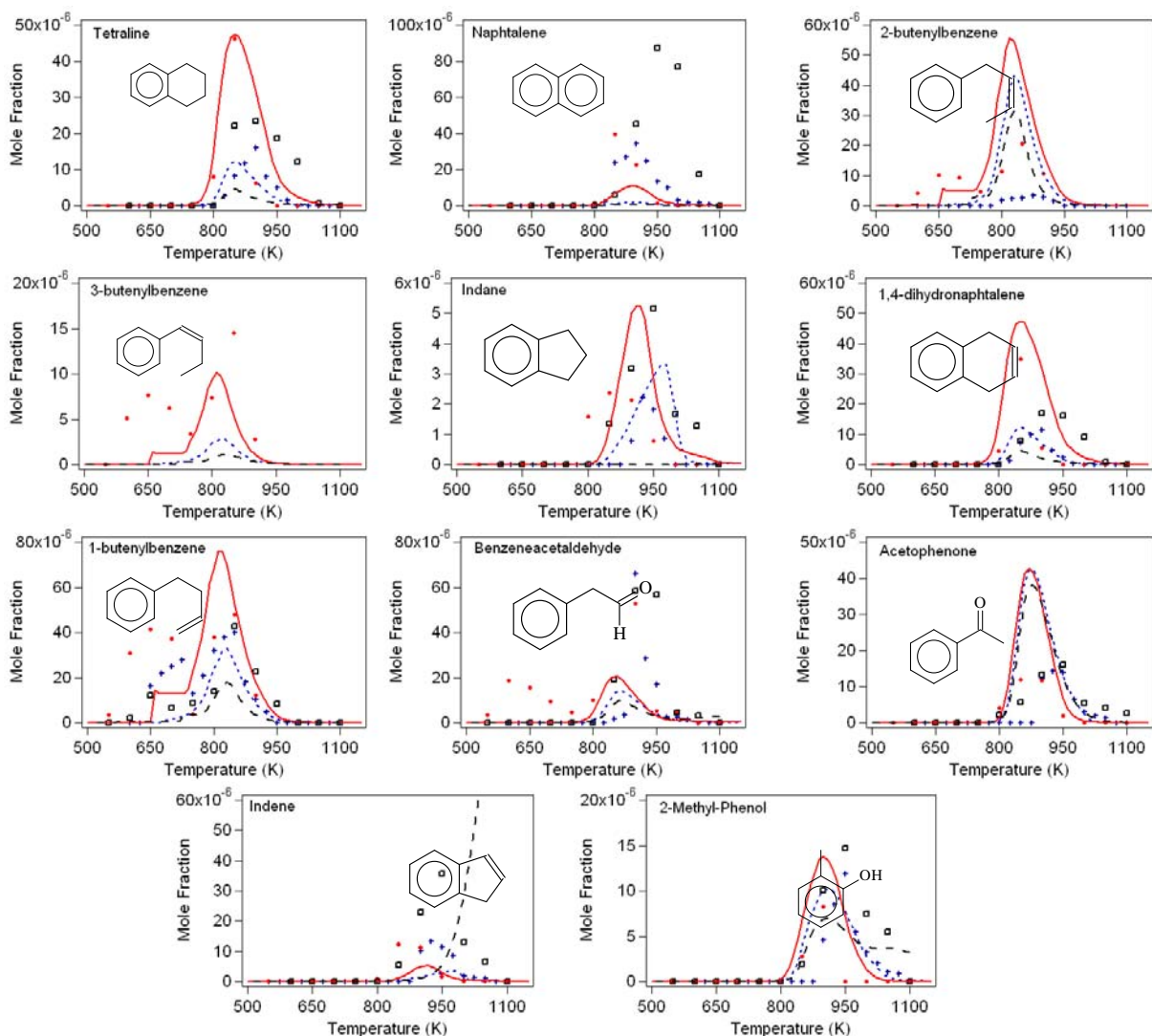


Fig. 9. Jet-stirred reactor ($P = 1.06$ bar): experimental and simulated mole fractions versus temperature for *n*-butylbenzene/oxygen/argon mixtures oxidation at a residence time of 2 s and for an inlet fuel mole fraction of 0.4% and equivalence ratios from 0.25 to 2. Points are experiments and lines simulations. $\Phi = 0.25$: circles and full line; $\Phi = 1$: cross and broken line; $\Phi = 2$: squares and large broken line.

In this study, the same major species have been analyzed as detected by Diévar et al. [17]. Allene, propyne, 1-butene, and 1,3-butadiene were not quantified by Diévar et al. [17], and among the aromatic compounds quantified here, only benzene, toluene, styrene, propenylbenzene, benzaldehyde, and naphthalene were also reported by Diévar et al. [17].

Note that it was not possible to quantify the formation of cyclic ethers, ketones and aldehydes with the same skeleton as the reactant, such as those presented in Table 1. This is due to the fact that *n*-butylbenzene is not very reactive in the low-temperature regime under the conditions of this study. However, we observed traces (amounts < 0.1 ppm) of 1-phenylbutan-1-one, 1-phenylbutan-2-one, 1-phenylbutan-3-one, 4-phenylbutanal, 3-phenyltetrahydrofuran, 2-ethyl-3-phenyloxirane, and 2-benzyl-3-methyloxirane. Below 1000 K, the carbon balance is better than 90%. At higher temperatures, larger deviations start to be observed due to the formation of heavy polyaromatic compounds and soot condensing directly at the reactor outlet, especially under rich conditions.

Figure 7 shows that the reactivity of *n*-butylbenzene versus temperature exhibits a slight NTC behavior, with maximum fuel conversion at 650 K. This is in agreement with the results obtained by Diévert et al. [17] under more dilute conditions but at higher pressure. As shown in Fig. 8, acetaldehyde and propanal are among the main species formed at low temperature, and it can be seen that the mole fraction profile of these species also exhibits NTC behavior. The leaner the mixture, the more marked the NTC behavior. Similarly to the results reported in the rapid compression machine, the major aromatic products are styrene (Fig. 8) and benzaldehyde (Fig. 8). NTC behavior is also observed for benzaldehyde, benzeneacetaldehyde (Fig. 9), and butenylbenzenes (Fig. 9).

3. Description of the reaction mechanism

The mechanism described in this section to simulate the low-temperature oxidation of *n*-butylbenzene is an extension of that proposed by Pousse et al. [7] to simulate the species profiles measured in a lean laminar premixed methane flame doped with this aromatic reactant. The reactions specific to the low temperature have been mainly written following the rules taken into account during the automatic generation of mechanisms for the oxidation of alkanes and alkenes by the software EXGAS developed in our laboratory [18], [19], [21] and [27]. The mechanism consists of 393 species in 2303 reactions. Files including this mechanism and the related transport data formatted to be used with CHEMKIN software [28] are available as Supplementary material.

Thermochemical data were mainly estimated by the software THERGAS developed in our laboratory [29], which is based on the group additivity methods proposed by Benson [30], apart from the heat of formation of some species (see comments in the provided mechanism), which were taken from Burcat and Ruscic [31] (for biaromatic species) or reevaluated using quantum calculations performed by Gaussian03 [32] at the CBS-QB3 level of theory to calculate energies [33].

The reversible reaction $R + O_2 = RO_2$ is an important reaction route in the low-temperature oxidation of hydrocarbon radicals, and overall reactivity is very sensitive to its equilibrium constant. In the case of resonance-stabilized radicals, the reaction is less exothermic and the formation of peroxy radicals, a promoting step, is not favored. The thermochemical data for resonantly stabilized 4-phenylbut-4-yl radicals and of 4-phenylbut-4-ylperoxy radicals were calculated with THERGAS thanks to the group additivity method [30] and using bond dissociation energies proposed by Tsang [34] and Luo [35] to evaluate the enthalpy of the radical from that of the parent molecule. Since data for the group C–(Cb)–(C)–(O)–(H) involved in the 4-phenylbut-4-ylperoxy radical was not available in the literature, a first evaluation led to a heat of reaction for the peroxy radical formation as low as that of an allylic radical. In this case the low-temperature reactivity was too low. A new evaluation of the enthalpy of this group was performed to obtain a heat of reaction of -27.4 kcal/mol for the reaction of addition of 4-phenylbut-4-yl radicals to oxygen, which is consistent with the value used by Ribaucour et al. [16]. This datum can be compared with the heat of reaction of the addition of O_2 of an equivalent alkyl radical, hexan-2-yl, -36.1 kcal/mol, of an allylic radical, hex-1-en-3-yl, -19.8 kcal/mol, of a benzyl radical, -22.3 kcal/mol, from Murakami et al. [36]. This accounts for the lower stabilization of benzylic radical in comparison to an allylic radical.

As in the mechanism proposed by Pousse et al. [7], the present model includes the previous mechanisms to model the oxidation of C_3 – C_5 unsaturated hydrocarbons, which were built by the team of Nancy [37] (the rate constant newly proposed by Troe [38] for $H_2O_2 (+M) \leftrightarrow 2OH (+M)$ has been used), in addition to those for benzene [39] and toluene [20]. The recently revisited kinetic model for toluene oxidation proposed by Tian et al. [40] has also been considered. The present mechanism is divided into a primary mechanism including the reactions of *n*-butylbenzene and its radicals and a secondary mechanism involving the reactions of the primary products.

3.1. Primary mechanism to model the low-temperature oxidation of *n*-butylbenzene

n-Butylbenzene has been considered as undergoing oxidation by unimolecular and bimolecular initiations and ipso-additions of hydrogen and oxygen atoms and of hydroxyl, methyl, and HO₂ radicals, and also by hydrogen atom abstraction reactions by molecular oxygen and radicals present in significant concentrations at high temperature (O- and H-atoms, and OH, CH₃, and HO₂ radicals).

Pressure-dependent rate constants have been calculated for the four unimolecular decompositions involving the cleavage of a C–C bond. The proposed rate parameters are given in Table 2. The high-pressure limit rate constants for these reactions were calculated based on microscopic reversibility, using an estimate of the rate constant in the reverse direction for radical–radical recombination. For all four reactions, an estimated rate constant of $1.2 \times 10^{13} \text{ cm}^3 \text{ mol}^{-1} \text{ s}^{-1}$ was used for radical recombination to form *n*-butylbenzene. A chemical activation formulation based on quantum Rice–Ramsperger–Kassel theory, as described by Dean [41] and [42] was then used together with the high-pressure limit expressions to develop pressure-dependent rate constants, which were fitted to a nine-parameter Troe formalism [43].

Table 2. Rate constants of the unimolecular decompositions of *n*-butylbenzene.

Reactions		A	n	E _a
ph#C4H9=ph#C3H6-1+CH3	k _∞	3.293x10 ²¹	-1.593	88,922
	k ₀	1.595x10 ³⁴	-5.630	54,290
	Troe	0.0241, 350.84, 1.19x10 ¹³ , 2317,1		
ph#C4H9=benzyl+nC3H7	k _∞	2.304x10 ²²	-1.586	77,244
	k ₀	2.308x10 ⁷⁵	-17.230	59,090
	Troe	0.003, 161.98, 171.13, 3417.5		
ph#C4H9=C6H5#+C4H9	k _∞	2.543x10 ²⁰	-1.239	102,520
	k ₀	1.268x10 ²⁰	-1.520	67,180
	Troe	0.1896, 442.79, 1.55x10 ¹⁰ , 2734.2		
ph#C4H9=C8H9#-1+C2H5	k _∞	1.144x10 ²⁴	-2.218	87,260
	k ₀	3.643x10 ³⁸	-6.790	52,480
	Troe	0.003, 337.69, 7.79x10 ¹² , 2258		

Note: Rate constants in the form $AT^n \exp(-E_a/RT)$ in cm³, mol, cal, and K units. The Troe parameters are listed in the order: a, T*, T**, T***.

Note that the only source available to estimate the rate constants for benzylic and derived radicals was by assuming a similar reactivity as for allylic and derived radicals. As differences certainly exist between the two types of radicals, some adjustments in rate parameters have been needed as detailed below. Without these adjustments, the reactivity in the JSR above 800 K was shifted by around 50 K toward lower temperatures and the ignition delay times in the RCM data were much overestimated for lean mixtures.

Concerning the reaction of *n*-butylbenzene molecules, the rate constant of the bimolecular initiation reactions with molecular oxygen considered by Pousse et al. [7] were adopted, which were taken from the correlation proposed by Ingham et al. [44]. Only the A factor of the bimolecular initiation leading to the resonantly stabilized 4-phenylbut-4-yl radicals was increased by a factor of 2.

In contrast to the mechanism of Pousse et al. [7], the reaction of the ipso-addition of an HO₂ radical to *n*-butylbenzene has been added, the products being butyl radicals and phenylhydroperoxide, which promptly decomposes to produce phenoxy and an OH radical. The rate constant used for this reaction was considered analogous to that of the similar reaction for toluene [45] (i.e., $4 \times 10^{11} \exp(-7096/T) \text{ cm}^3 \text{ mol}^{-1} \text{ s}^{-1}$).

Rate constants for H-atom abstractions were taken from Pousse et al. [7], with the exception of the metathesis reaction involving the OH radical and *n*-butylbenzene, yielding the resonantly stabilized 4-phenylbut-4-yl radical and 4-phenylbut-(3 to 1)-yl radicals, for which the A-factor was reduced by a factor of 3 from the value recommended by Pousse et al. [7]. The value for the formation of benzylic radicals was estimated by using the correlations proposed by Heyberger et al. [46] in the case of alkenes (abstraction of two allylic secondary H-atoms).

Compared to the mechanism of Pousse et al. [7], the H-atom abstraction reactions from *n*-butylbenzene by benzyl, phenyl, HCO, CH₂OH, CH₃O, C₂H₅, CH₃O₂, and phenylbutylperoxy (ph#C₄H₈OO, obtained by oxygen molecule addition to the phenylbutyl radicals (ph#C₄H₈)) radicals have been added, since these radicals can be present in large concentrations at low-temperature. The rate constants of these last reactions leading to the alkyl radicals and to the allylic radicals have been deduced from the correlations suggested by Buda et al. [18] and by Heyberger et al. [46], respectively. In the case of H-atom abstractions by HO₂ and peroxy radicals deriving from the reactant, the activation energy has been considered as being 2 kcal/mol lower than those proposed by Buda et al. [18] for alkanes.

High-temperature reactions of phenylbutyl radicals involved isomerizations, decompositions by breaking of a C–C bond to form styrene, ethylene, propene, and 1-butene as stable molecules, as well as the formation of butenylbenzenes by breaking a C–H bond or by oxidation with oxygen molecules. Termination steps were only written for the resonantly stabilized 4-phenylbut-4-yl radicals; combinations with HO₂ radicals led to the formation of phenylbutoxy radicals, combinations with CH₃ radicals produced 2-phenyl-*n*-pentane, and disproportionations with benzyl and allyl radicals gave but-2-enylbenzene, toluene, and propene, respectively.

The major changes compared to the high-temperature oxidation mechanism [7] concern phenylbutyl radicals, for which additions to molecular oxygen to form ph#C₄H₈OO have been included, as well as subsequent reactions; the isomerization reactions of ph#C₄H₈OO radicals to form hydroperoxyphenylbutyl (ph#C₄H₇OOH) radicals; the addition of ph#C₄H₇OOH radicals to molecular oxygen; and, finally, the formation of ketohydroperoxides through the isomerization and the decomposition of the products of the second addition to molecular oxygen. The rate constants of this series of reactions have been derived from the correlations proposed by Buda et al. [18]. The ph#C₄H₇OOH radicals decompose via β-scission or form cyclic ethers; the kinetic parameters of these reactions have been derived from the values proposed by Buda et al. [18], except from the resonantly stabilized ph#C₄H₇OOH radicals. The activation energy of the decomposition reaction of these radicals to form cyclic ethers has been considered to be 2 kcal/mol high than that for hydroperoxyalkyl radicals proposed by Buda et al. [18], due to the stabilization of these aromatic radicals.

The reactions of phenylbutyl radicals with molecular oxygen to give butenylbenzenes and HO₂ radicals are especially important under low-temperature conditions, as these reactions have a strong inhibiting effect on the reactivity. Kinetic parameters of these reactions have been suggested by Buda et al. [18] and by Heyberger et al. [19] for alkyl and alkenyl radicals, respectively. However, in the case of the oxidation reactions of 4-phenylbut-1-yl, 4-phenylbut-2-yl, and 4-phenylbut-3-yl radicals, the activation energies have been taken to be equal to 2.5 kcal/mol, compared to 5.0 kcal/mol for alkyl radicals. In the case of the resonantly stabilized 4-phenylbut-4-yl radical, the activation energy of the oxidation reaction has been estimated to be 2.0 kcal/mol lower than for the oxidation reactions of allylic type radicals.

A new termination step for the resonantly stabilized 4-phenylbut-4-yl radicals has been added; the combination with OH radicals to form phenylbutanol with a rate constant of $1.5 \times 10^{13} \text{ cm}^3 \text{ mol}^{-1} \text{ s}^{-1}$. The formation of 4,5-diphenyloctane and 1,2-diphenylpentane resulting from the combination of

4-phenylbut-4-yl radical with itself and benzyl radicals, respectively, has also been taken into account; the rate constant of these reactions has been assumed to be the same as for the recombination reaction of two benzyl radicals [20]. The formation of a hydroperoxide, 4-hydroperoxy-4-phenylbutane, has been written from the combination with HO₂ radicals. The rate constant of this reaction has been assumed to be $1.0 \times 10^{12} \text{ cm}^3 \text{ mol}^{-1} \text{ s}^{-1}$, by analogy with the reaction of benzyl [20]. The disproportionation reactions of HO₂ with ph#C4H8OO radicals have been also considered. The rate constant of the disproportionation reactions suggested by Buda et al. [18] has been adopted for this reaction.

3.2. Secondary mechanism to model the low-temperature oxidation of *n*-butylbenzene

The secondary mechanism proposed by Pousse et al. [7] includes the reactions of the three isomers of butenylbenzenes, allylbenzene, propylbenzene, 2-phenyl-*n*-pentane, and indane, as well as those of the derived products, namely butadienylbenzenes, and the bicyclic isomers of C₁₀H₁₀, indene and naphthalene.

The reactions of the newly considered primary products have been added in the secondary mechanism, i.e., the reactions of aromatic hydroperoxides, alkenes, cyclic ethers, aldehydes, alkanes, ketones, and alcohols. Lumped reactants are involved in the secondary mechanism to keep the model size reasonable [27]. For example, the description of ketohydroperoxide species has the unique formula ph#C3H6COOOH without distinction between the different isomers of the ketohydroperoxide species. Accordingly, although many different products can be obtained from ketohydroperoxide decomposition, the products have been assumed to be only benzaldehyde, carbon monoxide, and ethyl and OH radicals. This is because these species are the most reasonable ones in this decomposition reaction. The rate constants of the reaction of the primary products have been deduced from the correlations proposed by Biet et al. [21].

In addition to the above-mentioned reactions in the secondary mechanism, the addition reactions of the four alkenyl radicals, formed by H-atom abstraction from the isomers of butenylbenzenes, to molecular oxygen and the disproportionation reactions of the related alkenylperoxy radicals with HO₂ radical to form hydroperoxides have been considered. The rate constants, of these reactions have been deduced from the correlations proposed by Buda et al. [18]. The rate constants, of the cyclizations of phenylbutenyl and phenylpropenyl radicals to form C₁₀H₁₀ and indene, respectively, have been assumed to be the same as that proposed by Tsang et al. [47]. The mechanisms for the low-temperature oxidation of *n*-propane [18], propene [46], and *n*-butane [18] generated by EXGAS have been added.

4. Comparison between experimental results and modeling

All of these calculations have been performed using the CHEMKIN software package [28]. Simulation profiles have been compared to the experimental results recorded in an RCM, a ST, and a JSR, presented in this study, but are also compared to data already in the literature obtained in a JSR at 10 atm by Diévert and Dagaut [17], measured in a plug flow reactor at 1069 K and atmospheric pressure by Brezinsky et al. [11], and obtained in a low-pressure laminar premixed methane flame doped with *n*-butylbenzene by Pousse et al. [7]. Simulations were performed using the CHEMKIN suite of software [28]. Simulations of the RCM and ST data have been performed using the SENKIN software module assuming constant volume, adiabatic reactors. Simulations of the JSR and plug flow reactor data were performed using both the PSR and SENKIN modules, respectively, assuming homogeneous isothermal reactors. Simulations for laminar premixed flames were performed using the PREMIX module.

Results of simulations performed for some typical conditions using the model of Ribaucour et al. [16] and that of Diévarit et al. [17] are presented in Supplementary material.

4.1. Rapid compression machine experiments (present study)

Several experimental studies have demonstrated that the details of heat transfer in a rapid compression machine are quite complex, inducing possible gradients in the combustion chamber for low compression times [48]. However, previous work has shown that the hypothesis of adiabaticity for at least the core gas leads to good results for simulating ignition delay times of a wide range of fuels and for ignition delay times up to 150 ms obtained in the present apparatus (with a long compression time of 60 ms, which reduces turbulence) [18], [49] and [50]. For longer ignition delay times, heat losses have certainly some influence, and the hypothesis of adiabaticity leads to some underestimation of the delay times at the lowest temperatures, for which the largest uncertainty in the experimental results is also observed. Accordingly, the comparison between experimental and simulated results is displayed in Fig. 1 and Fig. 2 for equivalence ratios from 0.3 to 1. The agreement is overall rather good. The differences between prediction and experiments are at most a factor of 2 and the simulations agree reasonably well with the measurements for most of the experimental results. At equivalence ratios of 0.5 and 1.0, the NTC region and the cool flame delay times, as well as the magnitude of the NTC effect, are well predicted by the model. The model reproduces well decrease in reactivity when the mixture becomes leaner. While the agreement is not as good as that for richer mixtures, the slopes of the curves for the two leanest mixtures (equivalence ratios of 0.3 and 0.4) are mostly in agreement with the experimental results. The deviations observed for the leanest mixtures are certainly due to larger uncertainties in the models for the reactions of oxygenated species. As shown in the comparisons presented in the Supplementary material, the model of Ribaucour et al. [16] predicts well the ignition delay times obtained in the rapid compression machine, while that of Diévarit et al. [17] leads to significant deviations below 800 K, with especially strong NTC behavior predicted at $\Phi = 0.4$.

The model reproduces the formation of all the identified C_{10} aromatic species listed in Table 1, apart from ketones. Very small amounts of butadienylbenzene and dihydronaphthalene are predicted. Figure 10 presents the simulated evolutions of n-butylbenzene and of some major products computed for the following conditions: PTDC = 1.4 MPa, $T_c = 690$ K, $\Phi = 0.5$. The computed conversion of n-butylbenzene during the cool flame (more than 40%) is much larger than the experimental one (17%). However, the main aromatic products observed are the predicted ones: styrene (selectivity = 42%), benzaldehyde (selectivity = 22%), and butenylbenzenes (selectivity = 19%). Significant amounts of the C_{10} aromatic cyclic ethers, which have been experimentally detected, are also predicted. Note that in sampling, the whole reacting mixture, including the hot core gas and the colder boundary layer is extracted from the combustion chamber. This can partially explain the difference observed between simulations and the experimental concentration data; e.g., the simulated selectivity of benzaldehyde observed after the cool flame is about two times larger than that of styrene, while styrene is the major experimental product under these conditions.

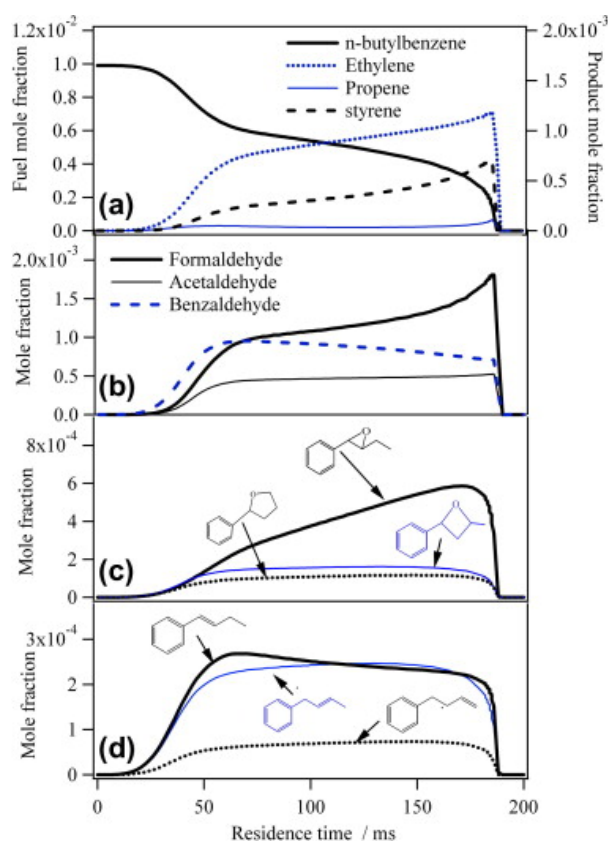


Fig. 10. Simulated profiles of fuel consumption and products formation under the conditions of Fig. 1a (PTDC = 1.4 MPa, $T_c = 690$ K, $\phi = 0.5$).

4.2. Shock tube experiments (present study)

The model was also tested against the experimental ignition delay times measured in a shock tube. Fig. 5 and Fig. 6 present ignition delay times versus inverse temperature for all of the experimental conditions. Figure 5 shows that while the agreement is good at atmospheric pressure, it deteriorates with increasing pressure, reaching a factor of about 4 at 30 atm for a temperature of 1000 K. As shown in Fig. 6, even if the agreement is not perfect, the model reproduces the main trend of the influence of the equivalence ratio, with the rich mixture being the most reactive at low temperature and high pressure and the least reactive at high temperature and low pressure. As shown in the comparisons presented in the Supplementary material, the model of Ribaucour et al. [16] strongly over predicts the ignition delay times obtained in the shock tube, while that of Diévert et al. [17] shows good agreement, even at high pressure.

4.3. Jet-stirred reactor experiments at atmospheric pressure (present study)

Comparisons of mole fraction measurements of species with simulations are shown in Fig. 7, Fig. 8 and Fig. 9. The agreement is mostly good for all the species analyzed; C_1 – C_4 hydrocarbons, small oxygenated compounds, aromatic species, and aromatics with an oxygen atom. For the rich mixture, the model over predicts the formation of most hydrocarbons above 950 K. This is due to the fact that the formation of large polycyclic hydrocarbons and soot was not taken into account in our model, while some experimental evidence of the formation of heavy compounds was found under these conditions. It is important to note that the model shows only negligible reactivity at temperatures below 800 K, while slight but noticeable reactivity is observed experimentally. The underestimation of reactivity by the model below 800 K leads to under prediction of the formation of all important low-temperature intermediates, such as acetaldehyde, propene, propanal, styrene, benzaldehyde, and benzeneacetaldehyde.

As shown in the comparisons presented in the Supplementary material, while both include low-temperature pathways, the models of Ribaucour et al. [16] and Diévert et al. [17] neither show any low-temperature reactivity under these conditions. They also significantly over predict the reactivity at temperatures above 800 K.

4.4. Jet-stirred reactor experiments at 10 bar

Diévert and Dagaut [17] have studied the oxidation of *n*-butylbenzene in a jet-stirred reactor at 10 atm under dilute conditions (1000 ppm of *n*-butylbenzene), over the low- and high-temperature range 550–1180 K and variable equivalence ratios (0.25, 0.5, 1.0, and 1.5). Figure 11 presents the simulated evolution of fuel and formaldehyde mole fractions (a good indicator of low-temperature reactivity) with inlet temperature for the four equivalence ratios studied. Under these conditions, for the lean mixtures, significant low-temperature reactivity is well predicted by the model, in agreement with the experimental results, but it is still too low compared to the experimental one, as shown for atmospheric-pressure data. As shown in the comparisons presented in the Supplementary material, the models of Ribaucour et al. [16] and Diévert et al. [17] significantly over predict the reactivity over the temperature range studied.

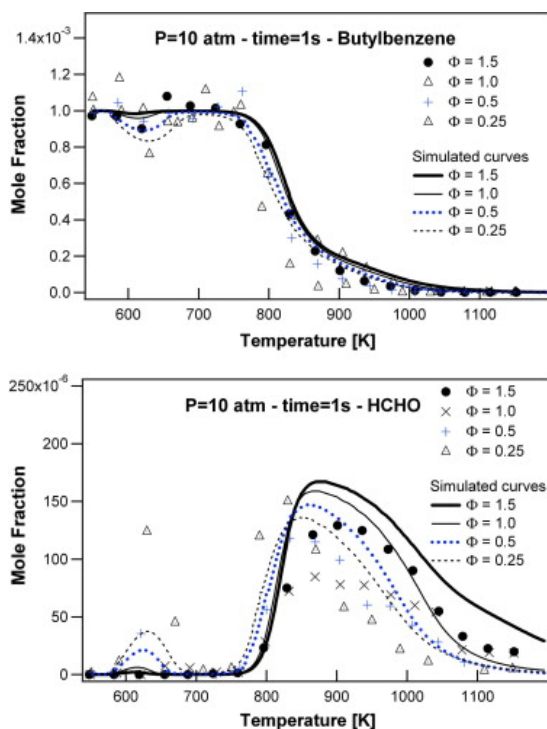


Fig. 11. Jet-stirred reactor ($P = 10$ bar): mole fractions of fuel and of formaldehyde (equivalence ratios of $\Phi = 0.25, 0.5, 1,$ and 1.5 , initial *n*-butylbenzene mole fraction of 1000 ppm, residence time of 1 s). The data (symbols from [17]) are compared to the simulations (lines).

Figure 12 presents mole fraction profiles for the main products at $\Phi = 0.25$ and at $\Phi = 1.5$ and shows that reasonable agreement is obtained. The same level of agreement can be observed for the two other equivalence ratios at $\Phi = 0.5$ and 1.0 in between.

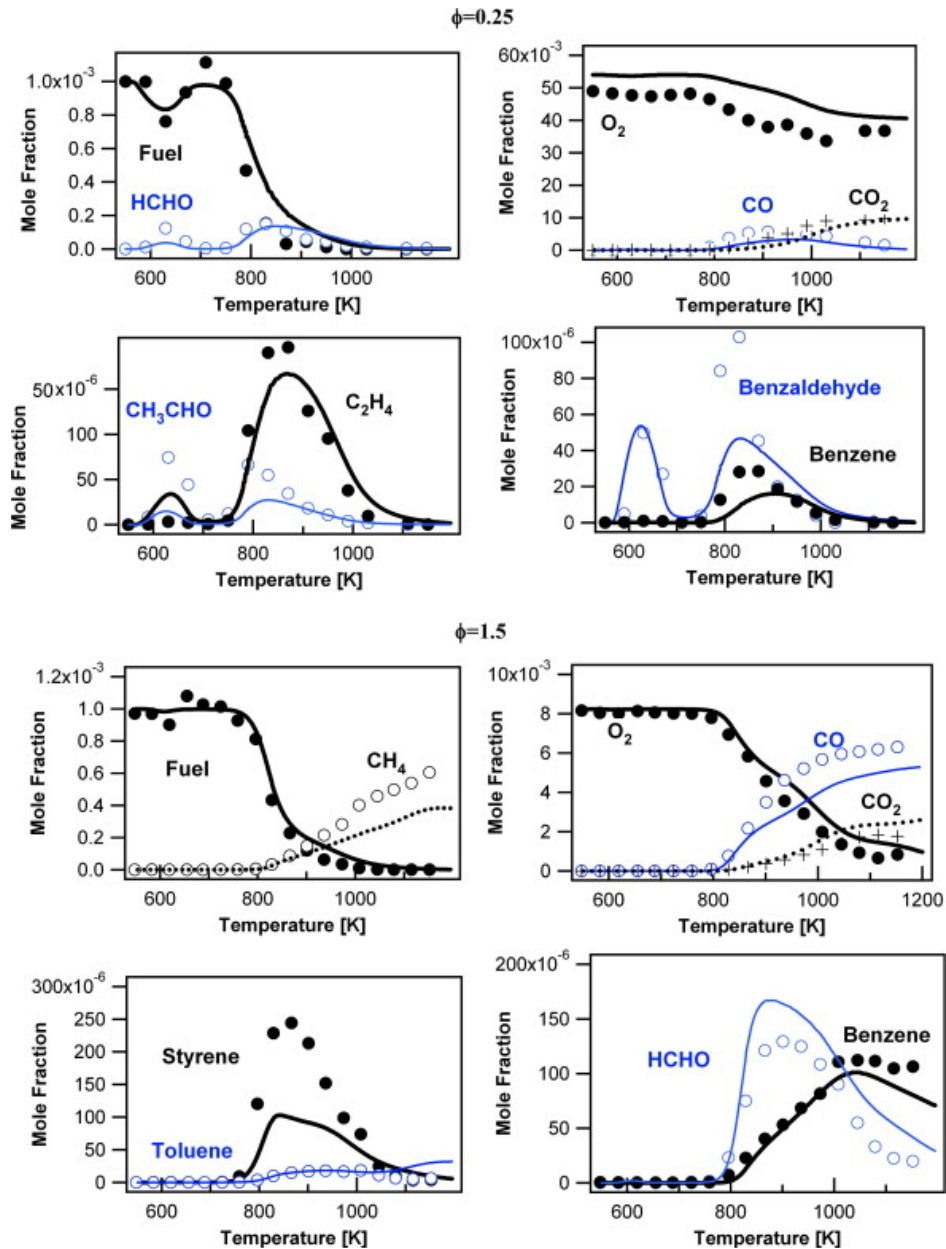


Fig. 12. Jet-stirred reactor ($P = 10$ bar): main product mole fractions for equivalence ratios of 0.25 and 1.5 (initial *n*-butylbenzene mole fraction of 1000 ppm, residence time of 1 s). The data (symbols from [17]) are compared to the simulations (lines).

4.5. Plug-flow reactor

To extend the validity of the model, the results of Brezinsky et al. [11], which were obtained in a flow reactor at 1069 K and at atmospheric pressure, with nitrogen as the bath gas, for an initial concentration of *n*-butylbenzene of 620 ppm and for an equivalence ratio of 0.98 have also been simulated. No shift of the initial time was made in the simulations. Figure 13 displays comparisons between the experimental and computed mole fractions of reactants and some main products. This figure shows that globally good agreement is observed. The consumption of reactant is correctly reproduced, as well as the formation of the major products.

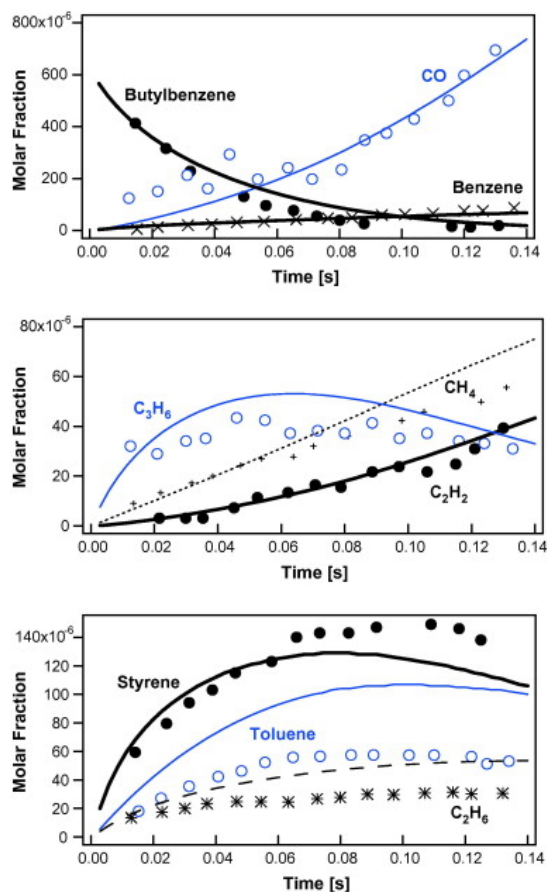


Fig. 13. Turbulent flow reactor (1 atm): main product mole fractions (temperature 1069 K, equivalence ratio $\Phi = 0.98$, initial *n*-butylbenzene mole fraction 620 ppm). The experimental results come from [11]. Points are experiments and lines simulations.

4.6. Laminar premixed flame

A laminar premixed flat flame has been stabilized in a burner by Pousse et al. [7] at 0.066 bar (50 Torr) with a gas flow rate of 5.44 L/min, corresponding to a gas velocity at the burner of 49.2 cm/s at 333 K and with mixtures containing 7.1% (molar) methane, 36.8% oxygen, and 0.96% *n*-butylbenzene, corresponding to an equivalence ratio of 0.74. Simulations were performed using as input the temperature profile given in Fig. 14 which was obtained as an average between the temperatures measured with and without the probe shifted 0.4 mm away from the burner surface to compensate for the perturbations induced by the quartz probe and the thermocouple. The convergence parameters (GRAD and CURV) were tightened until a solution independent of the grid was obtained. The transport data file is available as Supplementary material on the Website of this journal. Figure 14 shows the profiles of reactants and some representative species. Under low-pressure flame conditions the simulations were in good agreement with the data.

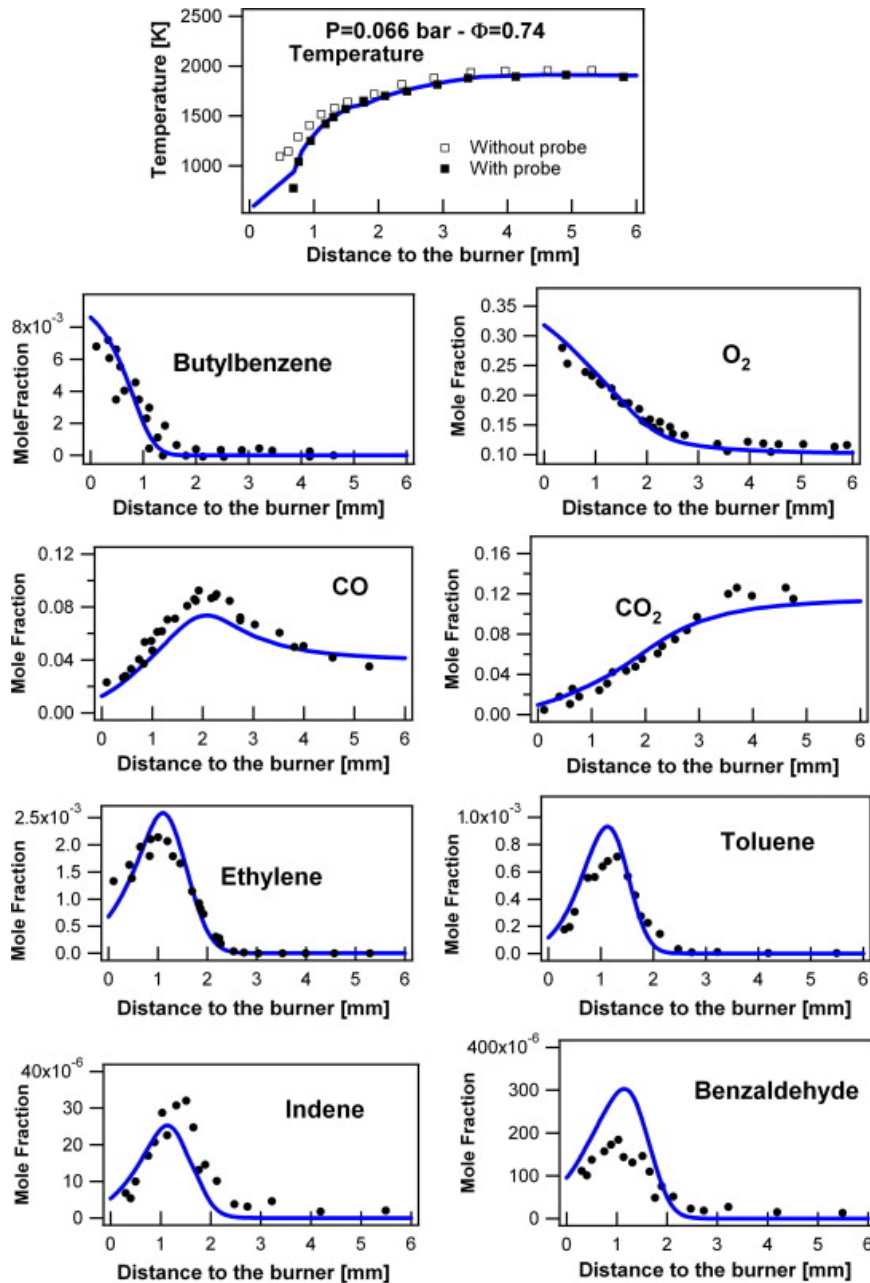


Fig. 14. Laminar premixed flame: temperature profiles and main product mole fractions ($P = 0.066$ bar, $\Phi = 0.74$, 7.1% (molar) methane, 36.8% oxygen and 0.96% *n*-butylbenzene, diluent = argon). The experimental results are issued from [7]. Points are experiments and lines simulations.

5. Discussion

As the constructed model correctly predicts ignition delay times measured in a rapid compression machine, we have used it to perform an analysis of the main reaction rates. In order to distinguish well the reactions responsible for the reactivity at low temperature, Fig. 15 shows a reaction rate analysis at a compressed gas temperature of 660 K for the conditions of Fig. 1c ($P = 14$ bar) and for a 10% conversion of *n*-butylbenzene (i.e., before the cool flame).

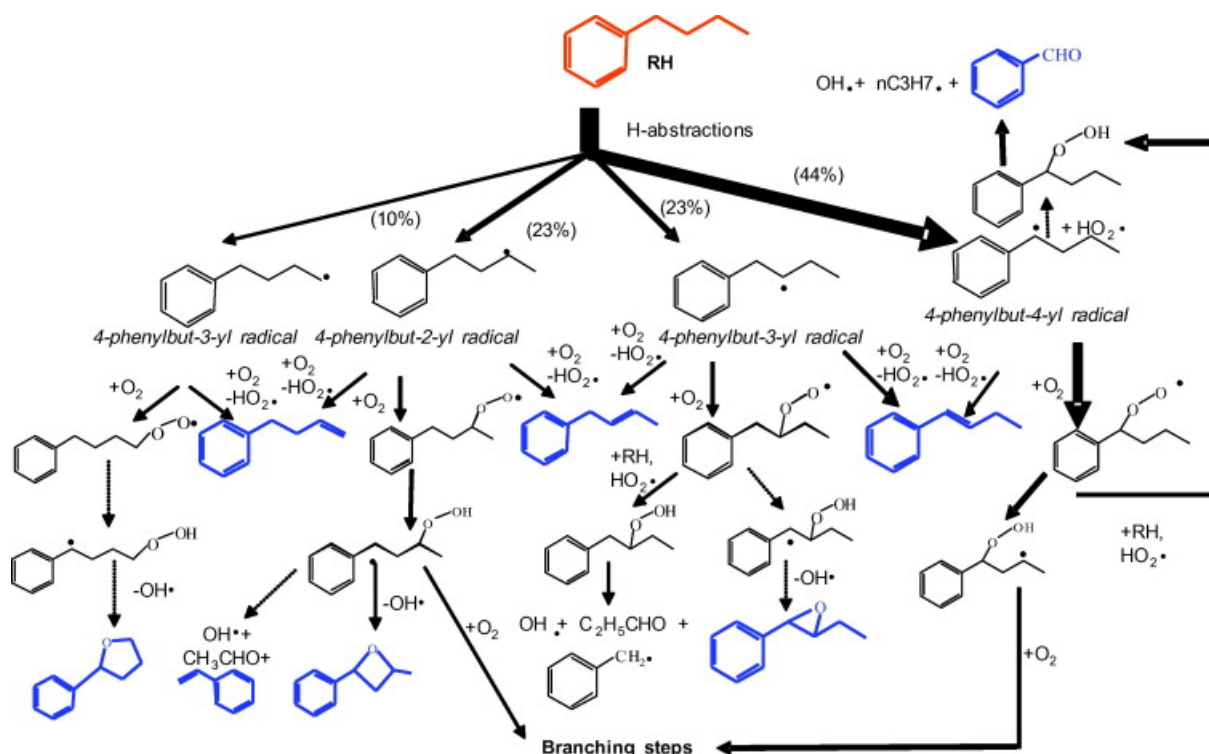


Fig. 15. Flow rate analysis for the low-temperature oxidation of *n*-butylbenzene under the conditions of Fig. 1c for a temperature after compression of 660 K, $P = 14$ bar, and 10% conversion of *n*-butylbenzene. Dotted arrows represent several successive elementary reactions. Compounds in bold are the main aromatic products (the names of the C_{10+} compounds are given in Table 1).

Under these conditions, 44% of *n*-butylbenzene (ph#C4H9) is consumed via hydrogen atom abstractions to form resonantly stabilized 4-phenylbut-4-yl radicals (ph#C4H8X):



This pathway is the main channel consuming *n*-butylbenzene. Note that at this low temperature, H-atoms are abstracted not only by OH radicals (approximately 37%), as is usually the case for many hydrocarbons, but also by 4-phenylbut-4-ylperoxy and 4-phenylbut-3-ylperoxy radicals (approximately 10%). The other important channels consuming *n*-butylbenzene are H-atom abstractions to form the three alkyl phenylbutyl radicals, 4-phenylbut-1-yl (ph#C4H8-1), 4-phenylbut-2-yl (ph#C4H8-2), and 4-phenylbut-3-yl (ph#C4H8-3):



Following the formation of phenylbutyl radicals, their main consumption pathway is their addition to molecular oxygen to form phenylbutylperoxy radicals:



This reaction type accounts for approximately 91% of the consumption of the resonantly stabilized 4-phenylbut-4-yl radical, but is less important for alkyl radicals. Other important reactions of phenylbutyl radicals are the oxidation reactions to form HO_2 radicals and the three butenylbenzenes (lumped as ph#C4H7), which are among the major reaction products (Fig. 10d):



A minor channel consuming resonantly stabilized 4-phenylbut-4-yl radicals is their combination with HO₂ radicals to form 4-hydroperoxy-4-phenylbutane:



The decomposition of the phenylbutylhydroperoxide molecules so produced in what is a degenerate chain-branching reaction is responsible for approximately 25% of the formation of OH radicals.



This reaction, which enhances global reactivity, is an important source of benzaldehyde (ph#CHO), the main oxygenated aromatic compound formed during the oxidation of *n*-butylbenzene. It is also the major source of propene via the oxidation of *n*-propyl radicals.

As shown in Fig. 15, phenylbutylperoxy radicals mainly isomerize to form phenylhydroperoxybutyl radicals in the case of 4-phenylbut-1-ylperoxy and 4-phenylbut-2-ylperoxy radicals, while the formation of phenylbutylhydroperoxide molecules through the reactions of peroxy radicals with *n*-butylbenzene or with HO₂ radicals is the main channel in the case of 4-phenylbut-3-ylperoxy and 4-phenylbut-4-ylperoxy radicals. The decomposition of the hydroperoxide molecules deriving from 4-phenylbut-3-ylperoxy radicals (ph#C₄H₈-3-OOH) gives propionaldehyde, and hydroxyl and benzyl radicals (ph#CH₂), the main source of toluene:



The most abundant phenylhydroperoxybutyl radicals deriving from the abstraction of an alkylic H-atom decompose mainly to give OH radicals and the three following cyclic ethers: phenyltetrahydrofuran, methylphenyloxetane, and ethylphenyloxirane (see Fig. 10d). These channels are responsible for approximately 25% of the formation of OH radicals. 4-Phenyl-2-hydroperoxy-but-4-yl radicals can also decompose by β-scission to form styrene, acetaldehyde, and OH radicals. Styrene is also one of the major products under the conditions of this study.

4-Phenyl-4-hydroperoxybut-2-yl radicals, which derive from the resonantly stabilized phenylbutyl radicals, mainly add to the molecular oxygen and ultimately lead to OH radicals and ketohydroperoxides which decompose, through a degenerate branched chain reaction, to form carbon monoxide, benzaldehyde, and OH and ethyl radicals. This series of reactions is the most important source of OH radicals (30% of the formation of this radical). Note that, while the second addition to molecular oxygen is also important in the consumption of 4-phenyl-2-hydroperoxybut-4-yl radicals, the formation of the ketohydroperoxide and the related degenerate branched-chain reaction mainly derive from the addition to molecular oxygen of the allylic type phenylbutyl radicals.

Figure 16 presents the flow rate analysis, focusing on the stabilized 4-phenylbut-4-yl radicals (ph#C₄H₈X) under the same conditions of Fig. 15 but at 660 (Fig. 16a), 829 (Fig. 16b), and 1000 K (Fig. 16c). It is interesting to note that at low temperature, the main channel consuming these radicals (91%) is the molecular oxygen addition reaction (Reaction (5)). At 829 K, the oxidation reaction (yielding butenylbenzene and HO₂ radicals, Reaction (6)) becomes more important (58%) and is a reason for the appearance of the NTC region. At 1000 K, the oxygen addition reaction becomes negligible to the benefit of the β-scission reaction which is a source of styrene (ph#C₂H₃):

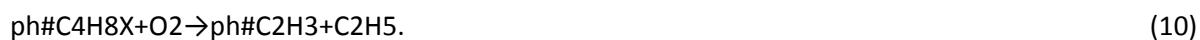


Figure 17 presents a sensitivity analysis of the addition reactions to molecular oxygen of each phenylbutyl radicals. This analysis was performed under the conditions of Fig. 1a by removing each reaction under investigation in turn. In the case of 4-phenylbut-1-yl radicals, the evolution of ignition delay times with temperature is almost the same as with the full mechanism. However, in the case of 4-phenylbut-2-yl and 4-phenylbut-3-yl radicals, the ignition delay times become longer over the whole temperature range compared to those computed with the full mechanism. In the case of allylic 4-phenylbut-4-yl (ph#C4H8X) radicals, ignition delay times are considerably longer and the evolution with temperature is drastically changed. This highlights the important role played by the addition to molecular oxygen of resonance-stabilized 4-phenylbut-4-yl radicals, as shown by the reaction rate analysis in Fig. 15. This feature is very different from what is usually observed for the addition reactions to molecular oxygen of other types of resonantly stabilized radicals, such as allyl [19] and benzyl [20] radicals. In these cases, the equilibrium constant is less favorable to the formation of peroxy radicals, as discussed above. The lack of easy isomerization reactions also displaces the equilibrium toward the reactants, while the longer alkyl chain in 4-phenylbut-4-yl radicals allows easy isomerizations, yielding hydroperoxy radicals, which compete with the backward decomposition giving $R + O_2$.

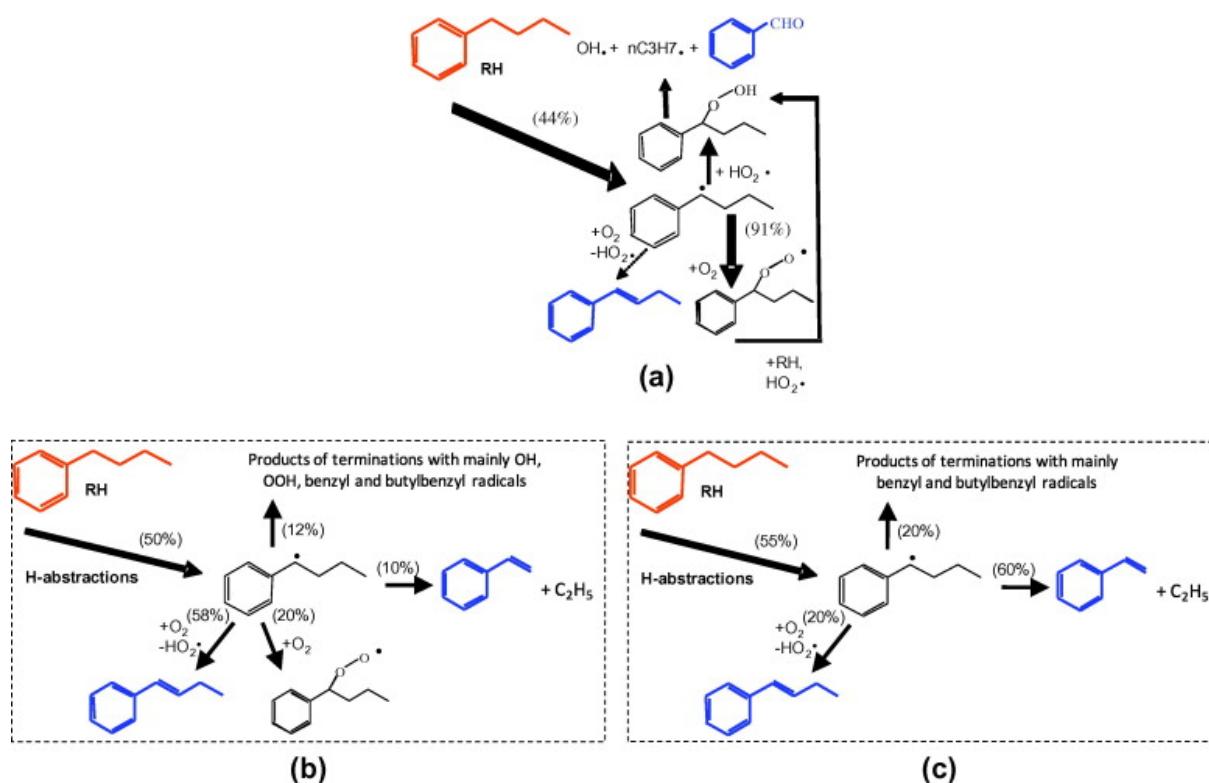


Fig. 16. Flow rate analysis for the low temperature oxidation of *n*-butylbenzene under the conditions of Fig. 1c focused on 4-phenylbut-4-yl radical (ph#C4H8X) reactions. (a) Temperature after compression of 660 K, $P = 14$ bar and 10% conversion of *n*-butylbenzene; (b) same conditions with $T = 830$ K, (c) same conditions with $T = 1000$ K.

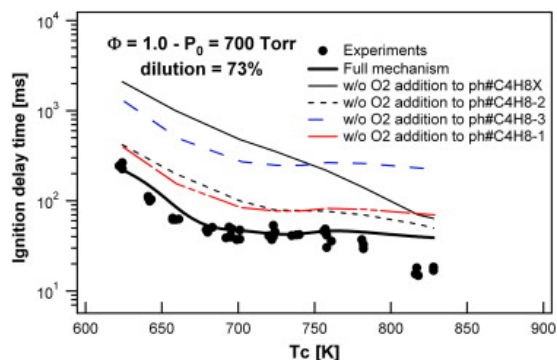


Fig. 17. Sensitivity analysis for the ignition delay times versus temperature under the conditions of Fig. 1c. Symbols correspond to experimental results and the line to simulation. The thick full line was obtained using the unchanged mechanism, the thin full line using a mechanism in which the addition of 4-phenylbut-4-yl radicals (ph#C4H8X) to oxygen was removed, the thin broken line using a mechanism in which the addition of 4-phenylbut-3-yl radicals (ph#C4H8-3) to oxygen was removed, the thin dotted line using a mechanism in which the addition of 4-phenylbut-2-yl radicals (ph#C4H8-2) to oxygen was removed, and the thin mixed line using a mechanism in which the addition of 4-phenylbut-1-yl radicals (ph#C4H8-1) to oxygen was removed.

6. Conclusions

New experimental measurements are presented for the autoignition of *n*-butylbenzene performed in a rapid compression machine (temperatures from 640 to 960 K, for three equivalence ratios, 0.3, 0.4, and 0.5) and in a shock tube (temperatures from 980 to 1740 K for four equivalence ratios, 0.3, 0.5, 1 and 2). The mole fraction profiles for reactants and products have been measured during the oxidation of *n*-butylbenzene in a jet-stirred reactor at temperature from 500 to 1100 K and for equivalence ratios of 0.25, 1, and 2. Even if the fuel mole fraction is four times that used by Diévar et al. in the same type of reactor but at 10 bar [17], the reactivity observed below 800 K is still rather weak.

A new detailed kinetic model has been also proposed. This mechanism has been constructed on the basis of the revisited high-temperature oxidation mechanism proposed by Pousse et al. [7] using the same rules of generation used in EXGAS for alkanes [18] to produce the low-temperature reactions. The new model reproduces satisfactorily most of the experimental results obtained in this study, as well as others in the literature.

Simulations have shown the considerable importance of the addition of allylic type phenyl butyl radicals to molecular oxygen, which promotes low-temperature reactivity, an unusual feature among unsaturated hydrocarbons.

Acknowledgments

This study has been supported by PSA Peugeot Citroën, by TOTAL and by SAUDI ARAMCO, and by the COST Action CM0901.

Supplementary material

Experimental data (JSR, RCM and ST); Butyl-benzene mechanism with transport data; Comparison with literature models

References

- [1] J.C. Guibet, *Fuels and Engines*, Publications de l'Institut Français du Pétrole, Editions Technip, Paris, 1999.
- [2] J.T. Farrell, N.P. Cernansky, F.L. Dryer, D.G. Friend, C.A. Hergart, C.K. Law, R.M. McDavid, C.J. Mueller, A.K. Patel, H. Pitsch, SAE Technical Paper 2007-01-0201.
- [3] F. Battin-Leclerc, *Prog. Energ. Combust. Sci*, 34 (2008), pp. 440–498
- [4] A. Ergut, Y.A. Levendis, H. Richter, J.B. Howard, J. Carlson, *Combust. Flame*, 151 (2007), pp. 173–195
- [5] S.P. Marshall, S. Taylor, C.R. Stone, T.J. Davies, R.F. Cracknell, *Combust. Flame*, 158 (2011), pp. 1920–1932
- [6] H. Anderson, C.S. McEnally, L.D. Pfefferle, *Proc. Combust. Inst.*, 28 (2000), pp. 2577–2583
- [7] E. Pousse, P.A. Glaude, R. Fournet, F. Battin-Leclerc, *Combust. Flame*, 156 (2009), pp. 954–974
- [8] T.A. Litzinger, K. Brezinsky, I. Glassman, *Combust. Flame*, 63 (1986), pp. 167–251
- [9] T.A. Litzinger, K. Brezinsky, I. Glassman, *Combust. Sci. Technol.*, 50 (1986), pp. 117–133
- [10] T.A. Litzinger, K. Brezinsky, I. Glassman, *J. Phys. Chem.*, 90 (1986), pp. 508–513
- [11] K. Brezinsky, G. Linteris, T.A. Litzinger, I. Glassman, *Proc. Combust. Inst.*, 21 (1986), pp. 833–840
- [12] P. Dagaut, A. Ristori, A. El Bakali, M. Cathonnet, *Fuel*, 81 (2002), pp. 173–184
- [13] H.P.S. Shen, M. Oehlschlaeger, *Combust. Flame*, 156 (2009), pp. 1053–1062
- [14] D. Darcy, C. Tobin, K. Yasunaga, J.M. Simmie, J. Würmel, W.K. Metcalfe, T. Niass, S.A. Syed, C.K. Westbrook, H.J. Curran, *Combust. Flame*, 159 (7) (2012) 2219–2232
- [15] A. Roubaud, R. Minetti, L.R. Sochet, *Combust. Flame*, 123 (2000), pp. 561–571
- [16] M. Ribaucour, A. Roubaud, R. Minetti, L.R. Sochet, *Proc. Combust. Inst.*, 28 (2000), pp. 1701–1707
- [17] P. Diévert, P. Dagaut, *Proc. Combust. Inst.*, 33 (2011), pp. 209–216
- [18] F. Buda, R. Bounaceur, V. Warth, P.A. Glaude, R. Fournet, F. Battin-Leclerc, *Combust. Flame*, 142 (2005), pp. 170–186
- [19] B. Heyberger, N. Belmekki, V. Conraud, P.A. Glaude, R. Fournet, F. Battin-Leclerc, *Int. J. Chem. Kinet.*, 34 (2002), pp. 666–677
- [20] R. Bounaceur, I. Da Costa, R. Fournet, F. Billaud, F. Battin-Leclerc, *Int. J. Chem. Kinet.*, 37 (2005), pp. 25–49
- [21] J. Biet, M.H. Hakka, V. Warth, P.A. Glaude, F. Battin-Leclerc, *Energy Fuels*, 22 (2008), pp. 2258–2269
- [22] M.H. Hakka, P.A. Glaude, O. Herbinet, F. Battin-Leclerc, *Combust. Flame*, 142 (2009), pp. 2129–2144
- [23] M. Carlier, C. Corre, R. Minetti, J.F. Pauwels, M. Ribaucour, L.R. Sochet, *Proc. Combust. Inst.*, 23 (1990), pp. 1753–1758
- [24] R. Minetti, M. Carlier, M. Ribaucour, E. Therssen, L.R. Sochet, *Combust. Flame*, 102 (1995), pp. 298–309
- [25] C. Morley, *Chemical Equilibria in Perfect Gases*, Version 0.76, 2004. <<http://www.gaseq.co.uk>>.
- [26] W.M. Haynes, *Handbook of Chemistry and Physics*, (91 ed.)CRC Press, Boca Raton, FL (2010) pp. 6–112
- [27] V. Warth, N. Stef, P.A. Glaude, F. Battin-Leclerc, G. Scacchi, G.M. Come, *Combust. Flame*, 114 (1998), pp. 81–102
- [28] R.J. Kee, F.M. Ruplay, J.A. Miller, Sandia Laboratories Report S 89-8009B, 1993.
- [29] C. Muller, V. Michel, G. Scacchi, G.M. Come, *J. Chem. Phys.*, 92 (1995), p. 1154
- [30] S.W. Benson, *Thermochemical Kinetics*, (second ed.)Wiley, New York (1976)
- [31] A. Burcat, B. Ruscic, Third Millennium Ideal Gas and Condensed Phase Thermochemical Database for Combustion with Updates from Active Thermochemical tables, 2008. <<http://garfield.Chem.elte.hu/Burcat/burcat.html>>.
- [32] Gaussian03, M.J. Frisch, G.W. Trucks, H.B. Schlegel, G.E. Scuseria, M.A. Robb, J.R. Cheeseman, J.A. Montgomery Jr., T. Vreven, K.N. Kudin, J.C. Burant, J.M. Millam, S.S. Iyengar, J. Tomasi, V. Barone,

- B. Mennucci, M. Cossi, G. Scalmani, N. Rega, G.A. Petersson, H. Nakatsuji, M. Hada, M. Ehara, K. Toyota, R. Fukuda, J. Hasegawa, M. Ishida, T. Nakajima, Y. Honda, O. Kitao, H. Nakai, M. Klene, X. Li, J.E. Knox, H.P. Hratchian, J.B. Cross, V. Bakken, C. Adamo, J. Jaramillo, R. Gomperts, R.E. Str atmann, O. Yazyev, A.J. Austin, R. Cammi, C. Pomelli, J.W. Ochterski, P.Y. Ayala, K. Morokuma, G.A. Voth, P. Salvador, J.J. Dannenberg, V.G. Zakrzewski, S. Dapprich, A.D. Daniels, M.C. Strain, O. Farkas, D.K. Malick, A.D. Rabuck, K. Raghavachari, J.B. Foresman, J.V. Ortiz, Q. Cui, A.G. Baboul, S. Clifford, J. Cioslowski, B.B. Stefanov, G. Liu, A. Liashenko, P. Piskorz, I. Komaromi, R.L. Martin, D.J. Fox, T. Keith, M.A. Al-Laham, C.Y. Peng, A. Nanayakkara, M. Challacombe, P.M.W. Gill, B. Johnson, W. Chen, M.W. Wong, C. Gonzalez, J. Pople, Gaussian03, Revision D02, Gaussian, Inc., Wallingford, CT, 2004.
- [33] J.A. Montgomery, M.J. Frisch, J.W. Ochterski, G.A. Petersson, *J. Chem. Phys.*, 110 (1999), pp. 2822–2827
- [34] W. Tsang, Heats of formation of organic free radicals by kinetic methods, J.A. Martinho Simoes, A. Greenberg, J.F. Liebman (Eds.), *Energetics of Organic Free Radicals*, Blackie Academic and Professional, London (1996), pp. 22–58
- [35] Y.R. Luo, *Handbook of Bond Dissociation Energies in Organic Compounds*, CRC Press, LLC (2003)
- [36] Y. Murakami, T. Oguchi, K. Hashimoto, Y. Nosaka, *J. Phys. Chem. A*, 111 (2007), pp. 13200–13208
- [37] H.A. Gueniche, J. Biet, P.A. Glaude, R. Fournet, F. Battin-Leclerc, *Fuel*, 88 (2009), pp. 1388–1393
- [38] J. Troe, *Combust. Flame*, 158 (2011), pp. 594–601
- [39] I. Da Costa, R. Fournet, F. Billaud, F. Battin-Leclerc, *Int. J. Chem. Kinet.*, 35 (2003), pp. 503–524
- [40] Z.Y. Tian, W.J. Pitz, R. Fournet, P.A. Glaude, F. Battin-Leclerc, *Proc. Combust. Inst.*, 33 (2011), pp. 233–241
- [41] A.M. Dean, *J. Phys. Chem.*, 89 (1985), pp. 4600–4608
- [42] A.M. Dean, *Combust. Sci. Technol.*, 80 (1991), pp. 63–85
- [43] R.G. Gilbert, K. Luther, J. Troe, *Ber. Bunsenges. Phys. Chem.*, 87 (1983), pp. 169–177
- [44] T. Ingham, R.W. Walker, R.E. Woolford, *Proc. Combust. Inst.*, 25 (1994), pp. 767–774
- [45] D.L. Baulch, C.J. Cobos, R.A. Cox, P. Frank, G. Hayman, Th. Just, J.A. Kerr, T. Murrells, M.J. Pilling, J. Troe, R.W. Walker, J. Warnatz, *J. Phys. Chem. Ref. Data*, 23 (1994), pp. 847–1033
- [46] B. Heyberger, F. Battin-Leclerc, V. Warth, R. Fournet, G.M. Come, G. Scacchi, *Combust. Flame*, 126 (2001), pp. 1780–1802
- [47] W. Tsang, *J. Phys. Chem. Ref. Data*, 20 (1991), pp. 221–273
- [48] J. Clarkson, J. Griffiths, J.P. MacNamara, B.J. Whitaker, *Combust. Flame*, 125 (2001), pp. 1162–1175
- [49] H.J. Curran, P. Gaffuri, W.J. Pitz, C.K. Westbrook, *Combust. Flame*, 114 (1998), pp. 77–149
- [50] M. Mehl, G. Vanhove, W.J. Pitz, E. Ranzi, *Combust. Flame*, 155 (2008), pp. 756–772